Internal Report
DESY F41-76/10
September 1976

Optical Excitation and Decay Processes in Rare Gas Solids

by

G. Zimmerer

To be published as a Chapter of Vol. 5 (Proceedings of the Intern. Summer School on Synchrotron Radiation Research, Alghero 1976) of the I.C.A.P. Series (Intern. College on Applied Physics, Catania, Italy), ed. by I.F. Quercia

OPTICAL EXCITATION AND DECAY PROCESSES IN RARE GAS SOLIDS

by

G. Zimmerer

II. Institut für Experimentalphysik der Universität Hamburg, 2000 Hamburg 50, Fed. Rep. Germany

1. INTRODUCTION

The basic fact which influences the physical properties of rare gases is the electronic configuration with closed shells: $1s^2$(He), $2s^22p^6$(Ne), $3s^23p^6$(Ar), $4s^24p^6$(Kr), and $5s^25p^6$(Xe). The interaction of ground state atoms is of van der Waals type leading to solidification only at low temperatures. Some properties characterizing rare gas solids (RGS) are summarized in Table 1. Different from all the other rare gases, He solidifies only under considerable pressure. It will be not discussed in this paper. Pure rare gases condense in a cubic close-packed (fcc) lattice [4]. RGS are in many respects the simplest crystals known to us. Often they are regarded as model substances for more complicated van der Waals crystals.

Table 1 Properties of RGS

	He	Ne	Ar	Kr	Xe
melting point (1) (deg K)	.95*	24.5	84.0	116.6	161.3
boiling point (1) (deg K)	4.215	27.2	87.5	120.9	166.1
nearest neighbour distance at 0 K (Å) (2)		3.13	3.76	4.01	4.35
ionization energy of free atom (eV) (3)	24.580	21.559	15.755	13.996	12.127

*at 26 atm

RGS gained much experimental and theoretical interest because of their outstanding properties indicated above. As for their optical properties, both experimental (5) and theoretical (6) results have been reviewed recently. RGS are perfect insulators. The band gap energies range from 9.3 eV (Xe) to 21.69 eV (Ne). Apart from these huge band gaps, the most striking feature of the optical properties is the existence of pronounced exciton series. Whereas the higher members of these series are Wannier like, the n = 1 members have a close correspondence to the first resonance lines of the free atoms and are more Frenkel type excitons. An interesting aspect from a theoretical point of view is the question whether the optical properties of RGS can be understood in the framework of band structure or more atomic like models.

The extreme properties of RGS make experimental investigations of the optical properties very complicated. They require a combination of vacuum ultraviolet (VUV) techniques, cryotechniques, and in several experiments ultra high vacuum (UHV) techniques. Ten and more years ago, optical measurements were confined to photon energies below ~ 14 eV because of the poor light sources available in the VUV region. A break-through was achieved, when in 1969, for the first time, synchrotron radiation was used for optical investigations of RGS (7). By use of the new source, since then all spectroscopic standard methods like absorption-, reflection-, and photoelectron spectroscopy (PES) have been applied to RGS.

In the meantime, rare gases gained enormous interest for application since it was demonstrated that they are well suited materials for the development of high power, tunable VUV lasers (8). Rare gas lasers are likely to play as important a role in VUV spectroscopy as dye lasers currently do at longer wave-lengths (9). Moreover, they may be important for the heating of high density plasmas for thermonuclear fusion applications (10). Consequently, the decay processes of excited electronic states of rare gases are

the decay processes of excited electronic states of rare gases are investigated since a few years. The decay processes not only include radiative decay of excited states but also scattering processes, the dynamics of excited states, energy transfer phenomena etc. In RGS, the dynamical behaviour of free excitons and exciton lattice interaction play a central role.

In the second chapter of this paper, the electronic structure of RGS as measured in primary excitation processes is briefly reviewed. In the third chapter, results on the decay processes of excited electronic states are presented.

2. ELECTRONIC STATES OF RARE GAS SOLIDS

2.1 General remarks

The electronic states of RGS have been investigated experimentally in the last two decades with conventional spectroscopic methods. From the Kramers Kronig analysis of absorption, reflection or energy loss data, the spectral dependence of the complex dielectric constant $\varepsilon(\hbar\omega) = \varepsilon_1(\hbar\omega) + i \cdot \varepsilon_2(\hbar\omega)$ was obtained. A complete compilation of the data is given in Ref. 5. Comparison with the optical data of gaseous rare gases showed that several features are similar in the gaseous and solid phase indicating an atomic like character of the electronic states of these simple solids. Other features of the optical spectra, however, are clearly related to molecular and solid state effect. Simultaneously to the experimental effort, the electronic states of RGS were investigated theoretically, especially by numerous band structure calculations (6). The essential characteristics of the RGS energy bands are very flat valence bands originating from the tightly bound outermost p electrons of the atoms and conduction bands with a nearly free electron behaviour. The valence bands are spin orbit split and distinguished by the total angular momentum $j = 3/2$ (upper valence band) and $j = 1/2$ (lower valence band) of the hole.

A serious difficulty in the understanding of the electronic states of RGS arises from the strong electron-hole interaction of excited states which is not neglegible in these perfect insulators. As already demonstrated in the early work of Baldini (12), electron-hole interaction results in prominent valence exciton series with binding energies two orders of magnitude larger than binding energies of excitons in semiconductors.

Up to now, there exists a controversal discussion whether the one-electron band structure approach is suited for a detailed understanding of the electronic states of RGS. Perhaps a more atomic or molecular like approach, which has successfully been adopted for the explanation of core excitations of a variety of solids (13,14), could lead to a better insight in the electronic states of RGS.

2.2 Excitons of bulk rare gas solids

The first investigation of the onset of absorption of solid Ar in the VUV was carried out by Nelson and Hartmann [15]. Later on, absorption measurements on solid Ar, Kr and Xe were performed by Schnepp and Dressler [16]. Since the detailed analysis of the absorption spectra of solid Ar, Kr, Xe for excitation energies up to 14 eV by Baldini [12] the number of investigations increased enormously. A survey on the onset of the optical spectra is given in Fig. 1. The imaginary part of the dielectric constant, $\varepsilon_2(\hbar\omega)$, is plotted as a function of excitation energy.

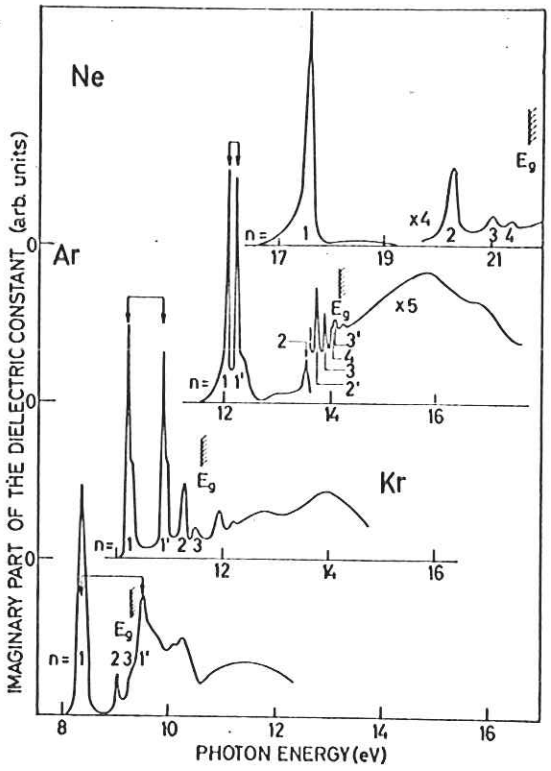

Fig. 1 Imaginary part of the dielectric constant of RGS. The References are given in the text. The temperatures of the measurements are: 5K (Ne); 10K (Ar); 20K (Kr); 20.4K (Xe)

$\varepsilon_2(\hbar\omega)$ was obtained from more recent reflection data by a Kramers Kronig analysis (Ne [17], Ar [18], Kr [19], Xe [20]). A detailed analysis of the optical data yields the following results:

(1) The pronounced structures at the onset of absorption can be classified into two exciton series which converge to the bottom of the conduction band at the center of the Brillonin zone, Γ. The two series are spin orbit split due to the different holes of the spin orbit split valence bands involved in the formation of the excitons. The nomenclature of the exciton series is $n = 1,2,3...$ for the $\Gamma(3/2)$ series and $n' = 1,2,3...$ (or sometimes $n = 1',2'...$) for the $\Gamma(1/2)$ series. n and n' are the main quantum numbers of the excitons. The numbers in the brackets give the total angular momenta of the holes.

(2) The excitons in RGS are neither of pure Wannier type nor of pure Frenkel type but of an intermediate type [6]. Only the excitons with $n > 1$, $n' > 1$ can be described by the Wannier formula

$$E_n = E_G - \frac{B}{n^2} \qquad (1)$$

where E_n means the excitation energy of the exciton with main quantum number n. E_G is the ionization limit, which is identical with the band gap, E_g, for the $\Gamma(3/2)$ series. B is the binding energy.

(3) The $n = 1$ and $n' = 1$ excitons show a more or less pronounced deviation from the Wannier formula. Their energies are close to the first $[np^6(^1S_o) \rightarrow np^5(^2P_{3/2})(n+1)s]$ and second $[np^6(^1S_o) \rightarrow np^5(^2P_{1/2})(n+1)s]$ resonance line of rare gas atoms [3].

In Fig. 1, the quantum numbers of the excitons and E_g are included. The splitting between the $n = 1$ and $n' = 1$ excitons is also indicated. This splitting, however, is not the most appropriate value for the spin orbit splitting because it is also influenced by exchange energy and slightly differs from the splitting of the ionization limits and of the $n = 2$, $n' = 2$... excitons. In solid Ne, spin orbit splitting is very small. It could be measured only recently [17] in the solid phase. The splitting increases via Ar, Kr to Xe. In solid Xe, it exceeds the binding energy of the $\Gamma(3/2)$ series. Therefore, the $\Gamma(1/2)$ series of Xe completely overlaps with the continuum of the $\Gamma(3/2)$ series. In Table 2 the newest values for the exciton energies, the binding energies and spin orbit splitting, Δ, are compiled. For solid Ar, Kr and Xe, the values are taken from Ref. 22. They stem from absorption measurements with a resolution which is by one to two orders of magnitude better than the line width of the excitons themselves. The values in brackets for $n = 1$ excitons are due to additional peaks which show up in reflection only on thick layers of RGS and which are not understood up to now.

From the Wannier character of the higher members of the exciton series, the band gap E_g, the binding energy B and the effective mass of conduction electrons, m_e^*, can be determined. E_g and B are obtained from a plot of E_n versus $1/n^2$ (examples are shown in Sec. 2.3). The binding energy of Wannier excitons is given (in the effective mass approximation) by

$$B = \frac{\mu^* e^4}{2\hbar^2 \varepsilon_o^2} \qquad (2)$$

where ε_o is the static electronic dielectric constant and μ^* the reduced effective mass of the exciton. Due to the flat valence bands, in RGS the effective mass of the holes, m_h^*, is much larger

Table 2 Experimental data of bound exciton states. All energies in eV; reduced effective masses in electron mass units. The spin orbit splitting, Δ, is compared with theoretical values (Δ_T) and atomic values (Δ_A). $E_{1,W}$ are the Wannier values for the n = 1 and n' = 1 excitons

	$Ne^{(17)}$	$Ar^{(22)}$		$Kr^{(22)}$		$Xe^{(22)}$	
n,n'		$\Gamma(3/2)$	$\Gamma(1/2)$	$\Gamma(3/2)$	$\Gamma(1/2)$	$\Gamma(3/2)$	$\Gamma(1/2)$
1	17.83*	12.059	12.236 (12.502)	10.173 (10.291)	10.855 (10.942)	8.37 (8.43)	9.508
2	20.38	13.565	13.749	11.232	11.920	9.072	
3	21.09	13.893	14.069	11.439	12.207	9.213	
4	21.38	13.969		11.516			
5	21.50						
$E_{1,W}$	16.44	11.793	12.021	10.082		8.311	
E_A**	16.67	11.624	11.828	10.033	10.644	8.437	9.571
E_G	21.69	14.155	14.325	11.612		9.326	
B	5.24	2.362	2.304	1.530		1.015	
Δ	~.1	.184		.688		1.3	
Δ_T		$.18^{(23)}$		$.7^{(23)}$; $.64^{(24)}$		$1.37^{(23)}$; $1.43^{(25)}$	
Δ_A	$.17^{(3)}$	$.177^{(3)}$		$.666^{(3)}$		$1.306^{(3)}$	
μ^*	$.6^{(17)}$	$.47^{(22)}$		$.40^{(22)}$		$.37^{(22)}$	
μ_T		$.45^{(26)}$; $.44^{(23)}$		$.36^{(26)}$; $.35^{(23)}$		$.30^{(23)}$	

*from reflection data

**E_A: energy of atomic $p^6 \rightarrow p^5 s(s')$ transitions (3)

than m_e^*. Therefore, $\mu^* \approx m_e^*$. Values are given in Table 2. They are in good agreement with results of band structure calculations (23,26). The n = 1 and n' = 1 excitons in RGS do not fit the Wannier formula but are blue shifted. In Table 2, the Wannier values for the n = 1 and n' = 1 excitons according to Eq. (1) are included. The shift is characterized by the "central cell correction" (11)

$$C = \frac{B_E - B}{B} \qquad (3)$$

B_E is the experimental binding energy of the n = 1 exciton and B is defined by Eq. (1).

The essential ingredient for the application of the Wannier model is a distance between the electron and the hole which is large compared with the lattice constant. A Wannier exciton is simply an interacting pair of point charges in a dielectric medium. For RGS n = 1 excitons the assumptions involved in the Wannier model are not valid. This is evident from a calculation of the exciton radii from the Wannier model:

$$r_n = \frac{\hbar^2 \varepsilon_o}{\mu^* e^2} \cdot n^2 \qquad (4)$$

The radii of the n = 1 excitons, r_1 = 1.1 Å (Ne), 1.8 Å (Ar), 2.5 Å (Kr), 3.2 Å (Xe) would be considerably smaller than the nearest neighbour distances (see Table 1).

The close correspondence between the n = 1 and n' = 1 excitons with the gas lines suggests an interpretation as Frenkel excitons, that means as excited atoms at a certain lattice site. The applicability of the Frenkel model to describe exciton states in RGS is reduced by the fact, that the involved electron states corresponding to the s-like conduction bands with their considerable width cannot be described by atomic-like wave functions (6).

The spin orbit splitting of the exciton series of solid Ar as well as the oscillator strengths of the n = 1 and n' = 1 excitons could be determined accurately enough (22) to calculate the energy of optically forbidden triplet excitons and the exchange energy in the framework of the theory of Onodera and Toyozawa (21). The valence band holes with j = 3/2, 1/2 couple together with the excited electron to exciton states with total angular momentum J = 2,1,1,0. Optically allowed excitons are those with J = 1 (n = 1 and n' = 1 excitons). Saile (22) found out that the forbidden J = 2 exciton has an energy ~30 meV below the energy of the n = 1 exciton. The J = 0 exciton state has an energy ~20 meV below the n' = 1 exciton. These results are important for Sec. 2.4. The J = 2,0 excitons could not be detected experimentally. The exchange energy deduced from the relative oscillator strength of the n = 1 and n' = 1 excitons (~1:1) has a value of ~23 meV which is by far smaller than the value of ~330 meV recently obtained by a theoretical calculation (27).

2.3 Impurity excitons in doped rare gas solids

A detailed insight into the nature of excitonic excitation of RGS can also be obtained by investigation of impurity absorption of doped RGS. In the work of Baldini (28) on the impurity absorption of RGS doped with rare gases several impurity absorption lines

showed up which (at least in the case solid Ar doped with Xe) seemed to fit a Wannier formula

$$E_n^i = E_G^i - \frac{B^i}{n^2} \qquad (5)$$

where E_n^i is the energy of impurity excitations, B^i the binding energy, and E_G^i the ionization limit.

A crucial test of the hydrogenic behaviour of impurity absorption lines which justifies their interpretation as impurity exciton series was given only recently by Pudewill et al [17]. It was possible to identify impurity exciton states of Ar, Kr, Xe in a Ne matrix up to n = 4 by an improved sensitivity of the measurements. Because in these systems the impurity excitons are found in

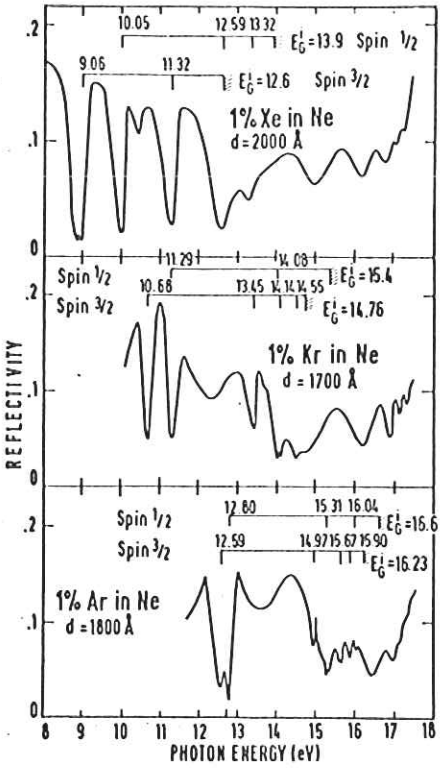

Fig. 2 Reflectance of Ne films doped with a) 1% Xe, d = 2000 Å; b) 1% Kr, d = 1700 Å; c) 1% Xe, d = 1800 Å. (d: thickness)

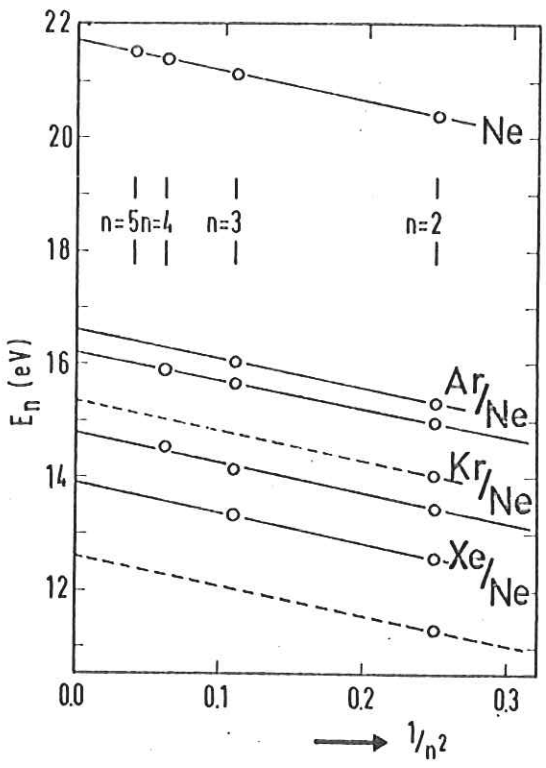

Fig. 3 Excitation energies of excitons in pure Ne and of the impurity states of Ar, Kr, and Xe in a Ne matrix plotted versus $1/n^2$

the transparency region of the matrix it is possible to detect impurity states in the reflectance of the substrate of the Ne sample. They show up as dips. In Fig. 2 the reflectivity of doped Ne films on a gold substrate is shown and the dips corresponding to the j = 3/2 and j = 1/2 impurity excitons and the ionization limits of both impurity exciton series

are indicated. In Table 3, the excitation energies E_n^i for Ar, Kr and Xe impurities in a Ne matrix are compiled. The early results of Baldini [28] are added in brackets. In Fig. 3, a plot of E_n^i versus $1/n^2$ is presented. The curve for the host excitons is included. The straight lines in Fig. 3 represent an excellent proof for the Wannier character of the host as well as impurity excitons with $n > 1$, $n' > 1$ in doped RGS. The binding energies of host and impurity exciton series showing up in the slope of the straight lines are nearly identical (see Table 3). In other words,

Table 3 Excitation energies (in eV) for Ar, Kr, and Xe impurities in a Ne matrix, the ionization limits E_G^i and the binding energies, B_i, of the impurity exciton series. The values are taken from Ref. 17. Values in brackets from Ref. 28

	Ar in Ne		Kr in Ne		Xe in Ne	
n, n'	j = 3/2	j = 1/2	j = 3/2	j = 1/2	j = 3/2	j = 1/2
1	12.59 (12.5)	12.80 (12.7)	10.68 (10.62)	11.29 (11.22)	9.06 (9.08)	10.05 (10.04)
2	14.97	15.31	13.45	14.06	11.32 (11.28)	12.59
3	15.67	16.04	14.14			13.32
4	15.90		14.55			
E_G^i	16.23	16.60	14.78			13.91
B^i	5.27	5.18	5.32			5.28

the identity of impurity excitons does not show up in the binding energy which is a property of the matrix exclusively. The individual nature of an impurity manifests itself only in the value for the ionization limit, the excitation energy of $n = 1$ and $n' = 1$ excitons and the spin orbit splitting of the series. The $n = 1$ and $n' = 1$ exciton energies deviate from the values predicted by the Wannier model in a similar way as in the pure substances. In RGS it makes no difference for the binding energies of excitons with $n > 1$ whether the hole involved is a hole in the flat valence bands or localized at an impurity. The electron involved in the formation of excitons can always be described in terms of wave functions of the conduction band of the matrix.

2.4 Surface states of rare gas solids

In former investigations of the excitonic structure of RGS sometimes weak peaks near the onset showed up which did not fit into the exciton series [29,30]. A very careful investigation of these effects carried out by Saile et al [22,21] demonstrated that surface states show up in the absorption spectra of solid Ar, Kr and Xe.

The essential experimental conditions under which the surface states can be detected are :

(1) Preparation of rare gas films and measurements must be carried out under UHV conditions (pressure $< 10^{-9}$ Torr).

(2) Measurements have to be carried out on very thin samples ($d \leq 500$ Å). Otherwise the amount of surface absorption is hidden in the background of the bulk absorption.

(3) The thickness of the layers must be controlled precisely in order to distinguish between interference effects and the absorption maxima.

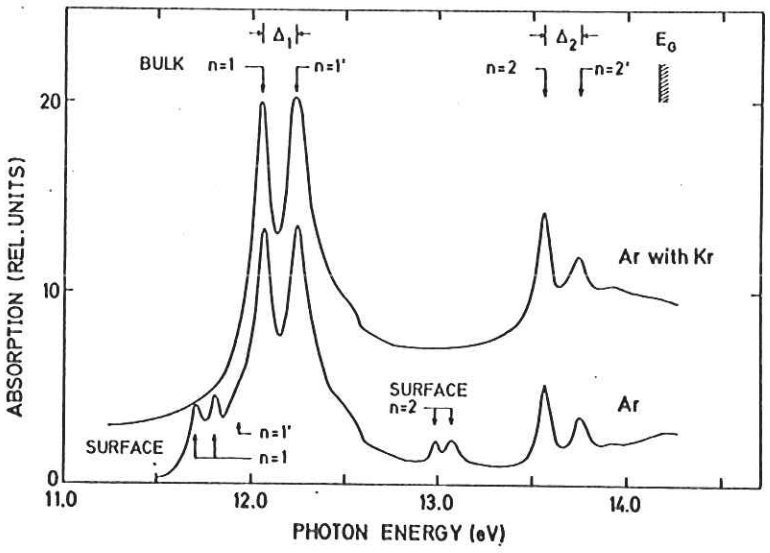

Fig. 4 Absorption spectrum of a clean Ar film (d=40 Å) and of the same film with a Kr coating. The surface and bulk excitons are labeled by their main quantum number n. Δ_1 and Δ_2 are the splittings resulting from the spin orbit split valence bands.

The influence of surface states on the absorption of solid Ar is demonstrated in Fig. 4. The lower curve shows the absorption of an Ar film (d = 40 Å) with a clean surface. Besides the bulk n = 1,2 and n' = 1,2 (n = 1',2' in the figure) excitons additional peaks show up at the low energy side of the n = 1 exciton and between the n' = 1 and n = 2 excitons. In contrast to measurements on thicker layers [22,30], in Fig. 4 the higher members of the exciton series do not show up because their diameter is comparable or even larger than the thickness of the Ar film (the diameter of the n = 3 exciton is 32 Å).

The Ar film covered with a thin Kr layer (upper curve) does not show the additional peaks which is a proof for the surface nature of these structures. The surface nature of the new peaks has been demonstrated even more convincingly in the case of Xe (Fig. 5). The full curve shows the bulk n = 1 exciton and the surface peak at its low energy side. The thin dashed line gives the absorption of the same film covered with Ar. The Ar overlayer can be removed by careful heating resulting in a reappearance of the surface peak (thick dashed curve).

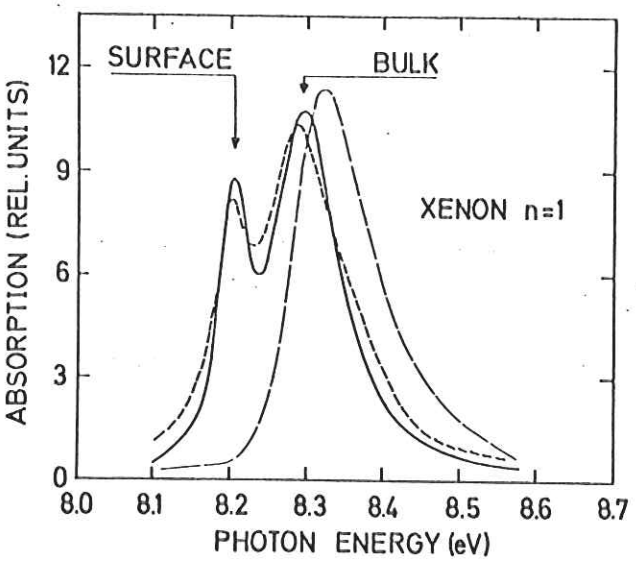

Fig. 5 Absorption of a Xe film of 30 Å thickness in the range of the n = 1 exciton. The full curve shows the surface and the bulk exciton, the thin dashed line gives the absorption of the same film with an Ar coating. The thick dashed line is obtained after removal of the Ar overlayer.

Table 4 Excitation energies of surface excitons of solid Ar, Kr and Xe (in eV). For comparison the values of the bulk excitons and of the bulk J = 2, 0 states are given. All values are taken from Ref. 22, 31.

	Ar	Kr	Xe
n = 1 (surface)	11.709 11.808	9.935 10.068	8.209
n = 1 (bulk)	12.059	10.173	8.37
n' = 1 (surface)	11.93	10.676	
n' = 1 (bulk)	12.236	10.855	
n = 2 (surface)	12.987 13.066	11.034	
n = 2 (bulk)	13.565	11.232	
n = 1 (J = 2)	~12.03		
n = 1 (J = 0)	~12.21		

The energies of the surface peaks of solid Ar, Kr, and Xe are summarized in Table 4 together with the energies of the n = 1 and n' = 1 bulk (transverse) excitons and of the J = 2,0 forbidden excitons. For the interpretation of the surface peaks of RGS different possibilities have been discussed by Saile [22]. The idea of surface exciton-polaritons [32] can be rejected because the measured peak energies are fairly smaller than the excitation energy of transverse excitons whereas surface exciton-polaritons are expected at the high energy side of transverse excitons in the gap between transverse and longitudinal excitons. The surface maxima also cannot be due to excitation of triplet excitons which could get allowed at the surface due to lowering of symmetry from O_h to C_{4v}.

There is a severe discrepancy between the measured and the calculated excitation energy (in the case of Ar, see Table 4).

In a crude model it was tried to interprete the new peaks as excitons the binding energy of which is changed by a modified dielectric screening in the region close to the surface. Averaging the dielectric constant of the bulk and the vacuum

$$\varepsilon_s = \frac{1}{2}(1 + \varepsilon_o) \qquad (6)$$

leads to a "surface dielectric constant", ε_s, which may be introduced into Eq. 2. Hereby it is assumed that the effective mass approximation is still valid for the surface peaks. This approximation may be applicable in the case of the large radius-excitons as for the n = 2 exciton in Kr, $r_{n=2}$ (bulk) = 10.5 Å. For solid Kr, qualitative agreement between the calculated modified n = 2 exciton and the measured n = 2 surface peak is obtained. In the case of solid Ar, this approach points to the right direction. For the n = 1 and n' = 1 surface peaks, this concept completely fails because of the small spacial extension of these excitations.

Recently, Wolff (33) interpreted the n = 1 and n' = 1 surface peaks as Frenkel type excitons. He analyzed group theoretically the splitting of the $^3P_{2,1,o}$ and $^1P_1$ states of the Ar $3p^54s$ configuration in the lowered symmetry at the surface (C_{4v}) as well as the selection rules for optical absorption. Under normal incidence only three transitions are allowed. Moreover, he calculated the multiplet splitting (intermediate coupling) of the $3p^54s$ configuration of an Ar atom embedded at the surface of an Ar crystal. The polarization of the nearest neighbours of the excited atom due to the localized hole was taken into account with the correct symmetry. The ansatz for the many body wave function of the $3p^54s$ configuration was split in a radial part and an angular part centered at the site of the excited atom. In the radial part of the wave function, parameters were introduced which allowed for a partial fitting to experimental results. If the splitting of the n = 1 surface states and the ratio of their oscillator strengths was used for the fitting procedure, the energetical position of the n' = 1 surface state as well as its oscillator strength could be predicted precisely by the calculation. Similar results have also been obtained for the Kr $4p^55s$ configuration.

2.5 Molecular type absorption and excitons in rare gas solids

A completely new aspect for the understanding of excitonic structures in the optical spectra of RGS has been given recently by Tilton et al (34,35) who measured the absorption of rare gas

impurities dissolved in alkali metal films for rare gas concentrations up to ~40% and compared them with the spectra of pure RGS.

The most interesting results can be summarized as follows:

(1) Sharp absorption peaks are found at excitation energies which are within .2 eV independent of the alkali metal hosts. They are only slightly blue shifted compared with the energies of n = 1 and n' = 1 excitons in pure RGS. In Fig. 6, the absorption of Xe dissolved in K is shown as an example (35).

(2) The absorption strength per impurity atom increases linearly with concentration (Xe and Kr in all alkali metals).

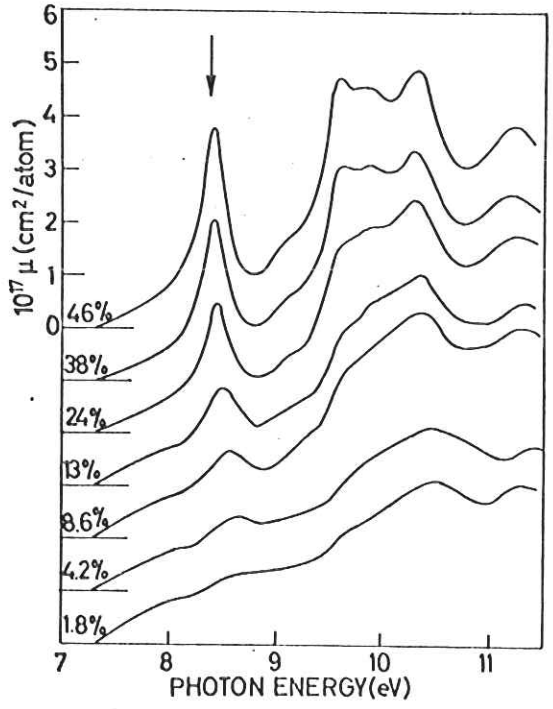

Fig. 6 The optical absorption per atom of Xe in potassium for various Xe concentrations (at%) at 7 K. The arrow marks the energy of the n = 1 exciton of solid Xe.

Not only the absorption of one kind of impurities in alkali metals but also the absorption of metal films doped with two different kinds of rare gas atoms was measured, e.g. of Ar/Xe dissolved in K (35). The absorption structures show a 1:1 correspondence to the Xe impurity exciton spectrum of Xe doped solid Ar. The height of absorption peaks is proportional to the product of the impurity concentrations.

The sharp absorption peaks are explained by molecular type absorption of pairs of rare gas atoms occupying neighboring sites in the lattice. The sharp features arising from pair bonds between rare gas atoms persist up to a concentration of ~40%. For such high concentrations, an impurity atom must have several neighbours of the same kind. Obviously these additional neighbours do not change the pair character of impurity absorption.

From these results, Tilton et al [34,35] conclude that the corresponding excitons in pure RGS or RGS doped with rare gases are due to molecular type of absorption and that a hole suddenly created in rare gas lattice cannot be confined to one lattice site. They propose that the description of impurity excitons in RGS should start with molecular wave functions of the diatomic rare gas molecule.

In this context it should be mentioned, that molecular type of absorption is well known from the gaseous phase of rare gases [36] and plays an important role for the luminescence properties of such systems [37].

2.6 Band to band transitions in rare gas solids

Though the optical properties of RGS have been investigated experimentally in the energy range of excitations from tightly bound valence band states to quasi-free conduction band states (see Ref. 5) we are far away from a detailed understanding of the features showing up in this part of the spectra. In Fig. 1, the imaginary part of the dielectric constant is included for the region of band to band transitions (Xe,Kr,Ar) above E_g. Several sharp and broad maxima show up in this part of the spectra. Though band structure calculations are available for all RGS [6] it is not possible to make an unambiguous assignment of structures in the optical spectra to structures in the joint density of states. In the case of heavy RGS (Kr and Xe) the situation is complicated by the fact that band to band transitions strongly overlap with the spin orbit split exciton series n' = 1,2... Moreover, it has been shown by Rössler et al [38] that electron-hole interaction for the continuum electron-hole states severely influences the spectral dependence of absorption. Due to Coulomb interaction, a considerable part of the oscillator strength is transferred from continuum states to bound exciton states (~30% for Xe, ~45% for Kr, ~63% for Ar). In the pair state continuum resonances are built up at the expence of the high density of non interacting pair states. Such resonances could be responsible for the rather sharp peaks found in the region of band to band transitions.

Similar to the atomic like interpretation of n = 1 and n' = 1 excitons in terms of $p^6 \rightarrow p^5s$ transitions, some of the structures in the continuum region have been explained by atomic $p^6 \rightarrow p^5d$ excitations in the case of solid Xe [25,39]. The pronounced 10.3 eV structure of Xe (see Fig. 1) closely corresponds to the atomic $p^6 \rightarrow p^5d$ lines at 9.9 eV, 10.4 eV [3] and does not vanish in liquid Xe [40] where a band structure based on long range order looses its meaning. Another interpretation for the pronounced 10.3 eV peak in the optical spectra of solid Xe has been given by Phillips [41]. The

10.3 eV maximum should be a hyperbolic exciton connected with the saddle point of the lowest conduction band at L. These informations all together may demonstrate that the interpretation of transitions in the continuum region of RGS either in a band structure model or in an atomic like model are still an open question.

2.7 Core excitations of rare gas solids

In the previous sections, excitations of the p-symmetric valence electrons of RGS have been discussed. The s-electrons of the same shell are only of minor importance in the solid because the lower conduction bands of RGS have s- and d-symmetric parts. Therefore, excitation of 5s(Xe), 4s(Kr), 3s(Ar) electrons only leads to weak structures. In the case of Ar and Ne, they are similar in the solid and the gaseous phase both as regards the weak oscillator strength and the asymmetric window shape [42]. With increasing excitation energy the next core electrons which come into play are the 4d(Xe), 3d(Kr) and 2p(Ar) electrons. Excitation of these electrons leads to pronounced structures in the optical spectra. In Fig. 7, a general view is given on the absorption of Xe from 8 eV to 1000 eV [5]. The solid curve between

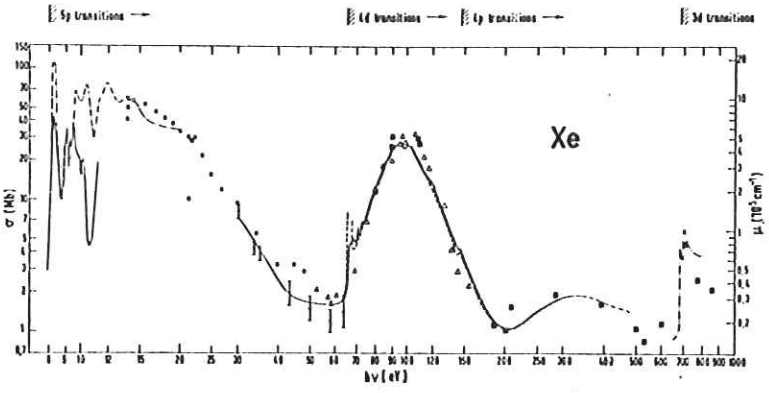

Fig. 7 Absorption coefficient of Xe. Below 20 eV (solid Xe): solid line from Ref. 44, 29; dashed-dotted curve from Ref. 12. 30 eV - 250 eV region: solid line (solid Xe) and dashed line (gaseous Xe) from Ref. 43. The points are from Ref. 45 (o), Ref. 46 (o), Ref. 47 ( ), and Ref. 48 ( ).

30 eV and 300 eV shows the first continuous measurement of the absorption of solid Xe in the region of 4d excitations [43]. It is compared with a measurement on gaseous Xe (dashed line) [43]. In both measurements, synchrotron radiation was used. The points represent different measurements with conventional light sources (x-ray tubes). In the region of Xe 4d excitations a close overall agreement between the optical spectra of the gaseous and the solid phase is observed. The same is true for Kr 3d [43] and Ar 2p [49] excitations. Striking differences between the gaseous and solid phase are observed in the onset region of core transitions. This is demonstrated in Fig. 8 which shows the onset of Xe 4d absorption in larger scale.

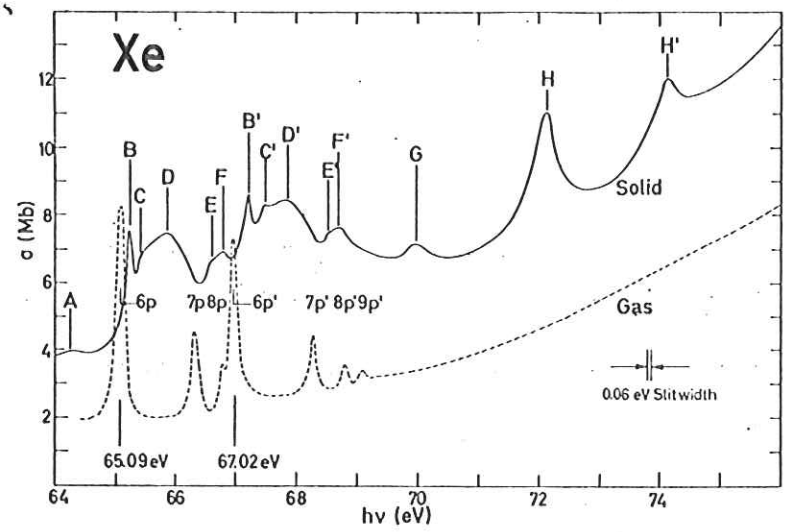

Fig. 8 Absorption coefficient of solid Xe and gaseous Xe (dashed curve) at the onset of 4d transitions. Spin orbit partners are denoted by primed and unprimed letters (43).

In the gaseous phase narrow absorption lines are observed. They are due to Rydberg series of the type $4d^{10}(^1S_o) \rightarrow 4d^9(^2D_{5/2;3/2})np$. The series are spin orbit split by the spin orbit splitting of the 4d hole. In the solid, rather broad as well as sharp (B,B'-maxima) structures are found. Rössler (50) has tried to interprete this region by transitions from the very flat core levels to conduction band states. In this case, the optical function if a superposition of the conduction band density of states with the spin-orbit splitting and degeneracy of the core levels taken into account.

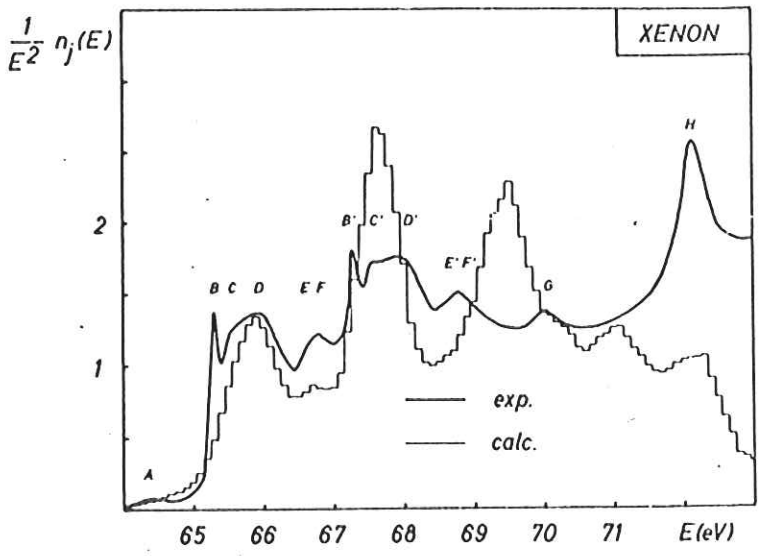

Fig. 9 Onset of absorption from Xe - 4d levels (43) in comparison with density of states calculations (50).

In Fig. 9 the measured absorption coefficient of the onset of Xe 4d transitions is compared with the calculated spectrum (50). Good agreement between both curves can be stated except of the narrow maxima B,B' which are explained as spin orbit split Frenkel type excitons. It is interesting to note that the one electron band structure is able to interprete the onset of core transitions quite well but fails in the interpretation of valence

excitations. This behaviour of RGS is not understood up to now. A good agreement between theory and experiment has also been obtained for the onset of Kr 3d absorption (50,26) and Ar 2p excitations (50).

The absorption spectra of core electrons above threshold with the great similarity in the gaseous and solid phase are interpreted in atomic models (51). This topic is beyond the scope of this paper.

2.8 Valence band structure of rare gas solids

In the past it turned out that not only optical spectroscopy but also photoelectron spectroscopy (PES) is an extremely useful tool for the investigation of the electronic structure of matter. In the case of insulators like RGS, charging of the samples is a severe problem for PES. Therefore, up to now, only thin evaporated layers of RGS have been investigated ($d \lesssim 1000$ Å). A strong effort was put into the study of energy transfer and relaxation phenomena (see chapter 3). From the electronic states of RGS the valence band structure has been deduced from energy distribution curves (EDC's). In Fig. 10, EDC's of solid Ne, Ar, Kr and Xe are presented (52, 53).

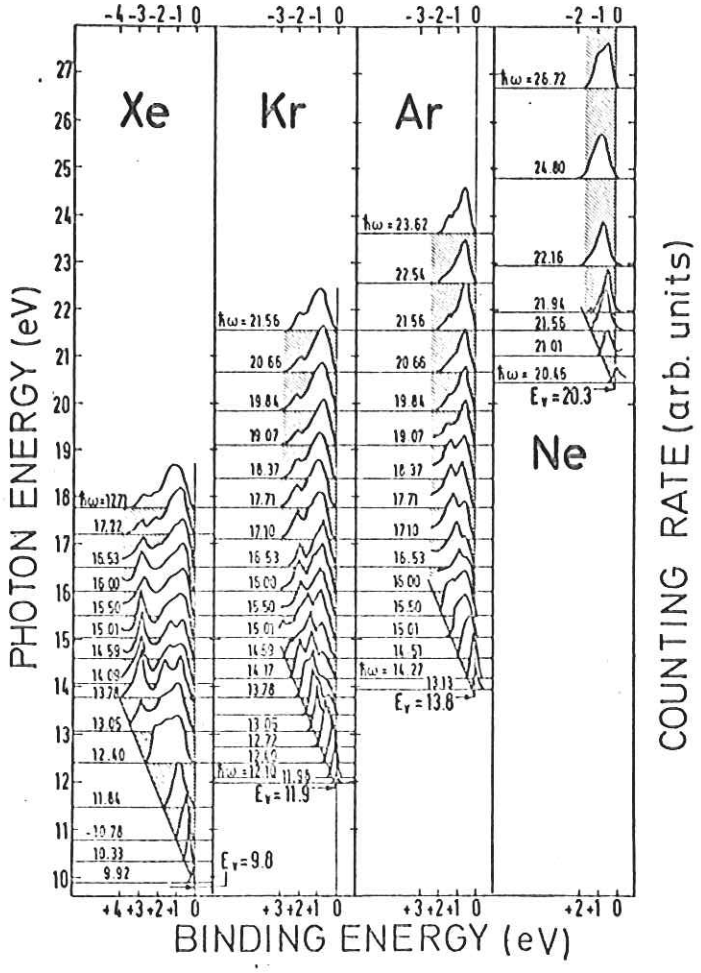

Fig. 10 EDC's for solid Ne, Ar, Kr, and Xe for various photon energies. Maximum counting rates are normalized except near threshold. The zero-count line for each curve is shifted upwards proportional to the exciting photon energy (52,53).

The excitation energies for the different curves are included. E_V means the energy of the vacuum level measured from the top of the valence band. The values of E_V are deduced from the EDC's. The excitation energies used are all below the onset of electron-electron scattering.

Above threshold, the width of the EDC's increases with increasing photon energy until the photon energy is sufficient to excite electrons from the bottom of the valence band. Then the width of the EDC's is independent of photon energy. It represents the total width of the valence bands (Ne: 1.3 eV, Ar: 1.7 eV, Kr: 2.3 eV, Xe: 3.0 eV) [52,53]. It considerably exceeds the spin orbit splitting of the valence bands and indicates the non-neglegible dispersion of the valence bands in $\vec{k}$-space.

In the EDC's of solid Xe, for excitation energies between 13 eV and 16 eV, three maxima can be clearly separated, the energy of which is independent of photon energy. Therefore they are attributed to density of states maxima of the valence bands. These density of states maxima stem from the region close to the Brilloun zone boundaries and indicate a considerable crystal field splitting of the $j = 3/2$ valence band. The two maxima with binding energies less than 2 eV originate from the upper ($j = 3/2$) valence bands. The third maximum stems from the lower ($j = 1/2$) valence band. In Kr, Ar, Ne a partial overlap of the three maxima is found because the spin orbit splitting and the dispersion of the bands decreases.

Recently [54] the experimental EDC's of Ar and Kr have been compared with different band structure calculations. It turned out that self consistent Hartree-Fock calculations corrected for both long range correlation effects (polarization) and short range effects (relaxation) are suited to obtain a reasonable agreement between theory and experiment.

3. DECAY OF EXCITED STATES OF RARE GAS SOLIDS

3.1 General remarks

The decay of excited states of RGS is not a single step process but contains different contributions. These may be generally divided into two groups:

(1) Radiative decay processes.

(2) Non - radiative decay processes.

The radiative decay processes are investigated by luminescence spectroscopy. Luminescence can be only measured from more or less long - lived intermediate states during the decay of electronic excitation. Obviously, these intermediate states are on the final

stage of a series of non - radiative cascading decay processes. This can be seen most convincingly from the fact, that luminescence spectra of RGS are nearly independent from the kind of excitation (see Sec. 3.2).

The non - radiative processes influence the quantum efficiency of luminescence and also show up in PES. Experimental investigations essentially need a tunable light source for the primary excitation. The different processes can only be unfolded if a well defined excited state is picked out by the excitation process itself. Therefore, among the various kinds of luminescence, photoluminescence is of special interest. In the case of RGS, photoluminescence as well as PES gained very much from the use of synchrotron radiation.

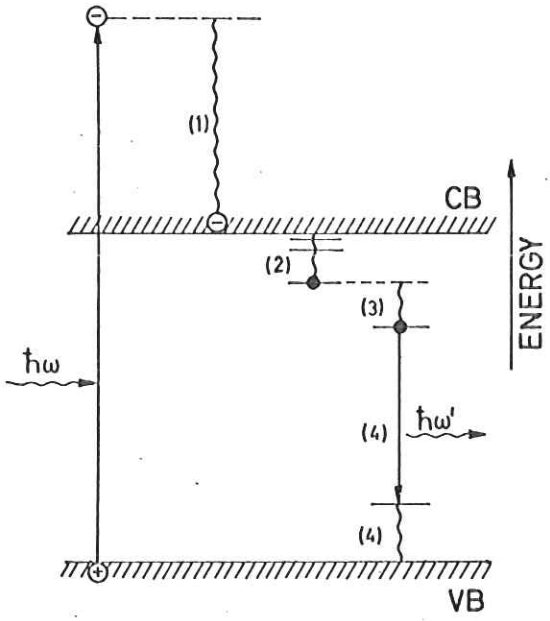

Fig. 11 Model for the decay of a conduction band state of RGS. $\hbar\omega$ is the excitation energy, $\hbar\omega'$ is the energy of luminescence photons. VB: valence band, CB: conduction band.

In Fig. 11, a schematic outline of the decay processes starting from a well defined excited conduction band state is given. In pure RGS we have to distinguish between four different steps:

(1) The high kinetic energy photoelectrons are slowed down by scattering (e.g. electron-phonon or electron-electron scattering).

(2) The slowed down electrons are captured by the holes and excitons are formed which relaxe to lower excitonic states.

(3) The excitons relaxe to localized states ("self trapping").

(4) The "self trapped exciton" (STE) decays radiatively to its ground state which is not in equilibrium with the lattice. Equilibrium with the lattice is obtained by non radiative relaxation of the STE ground state.

This model is very crude. Effects like self trapping of the hole before capture of the electron are neglected.

If we are dealing with doped RGS, energy transfer from the host to the guest may compete with all four steps. As acceptors not only doping atoms but also the substrate of the sample and atoms adsorbed at the surface play an important role. Energy transfer processes are influenced very much by the motion of free excitons in the lattice. All these processes can be investigated by measuring the following quantities:

(1) Luminescence spectra: the spectral distribution of luminescence light.

(2) Photoluminescence yield spectra (PLY) or excitation spectra. They give the efficiency of luminescence as a function of excitation energy.

(3) Energy distribution of photoelectrons (EDC's) under excitation with monochromatic light.

(4) Photoelectric yield curves (PEY) which give the efficiency of photoemission as a function of excitation energy.

(5) Time dependence of luminescence.

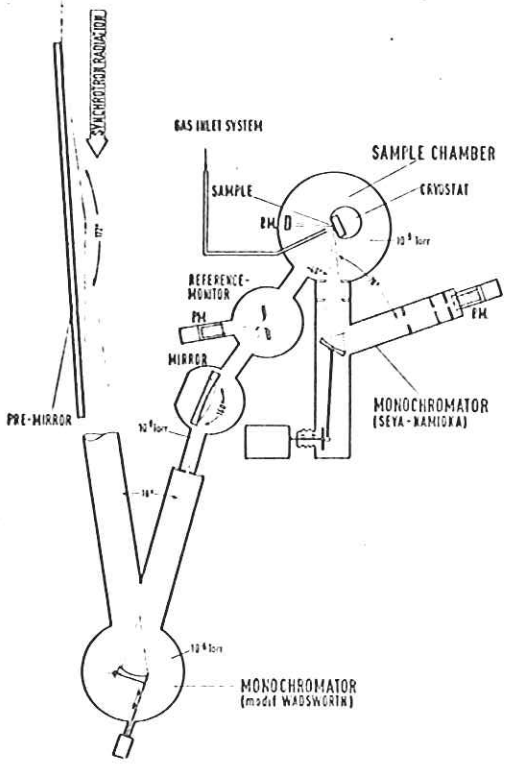

Fig. 12 Experimental set up for the investigation of RGS luminescence including PLY curves. Synchrotron radiation is used for primary excitation.

In Fig. 12, an experimental set-up for the investigation of RGS luminescence including PLY measurements is given (55). Synchrotron radiation is monochromatized by a near normal incidence monochromator. The monochromatized light is focused onto the sample. The focus serves as entrance slit of a Seya Namioka monochromator with which the emitted light is analyzed. This is an optimal fitting of an analyzing monochromator to the luminescing sample. Windows and

optical components to handle the luminescence light are avoided. Therefore, luminescence can be investigated from the far VUV (~30 eV) down to the visible. The samples are prepared by condensation of the rare gas on a gold-coated sapphire plate mounted on a He cryostat.

In order to measure a luminescence spectrum, the near normal incidence monochromator is fixed to a certain excitation energy and the Seya Namioka monochromator is scanned. PLY's of a certain luminescence band are obtained by fixing the Seya Namioka to the energy of the luminescence band and scanning the primary monochromator.

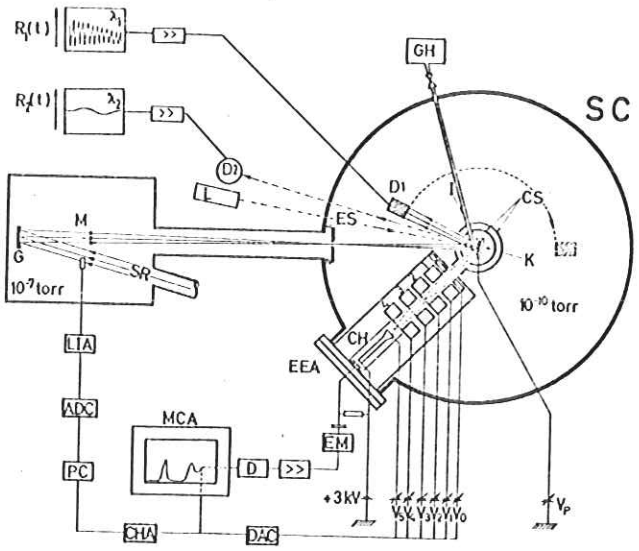

Fig. 13 Set up for simultaneous photoemission and reflection measurements (56). SR synchrotron light, M monochromator, EX exit slit, SC sample chamber, K cryostat with CS cooling shields, GH gas handling, I sample holder, EEA electron energy analyzer with CH channeltron, D1 measures the reflectance, with D2 the thickness of the samples is measured, L laser.

In Fig. 13, a typical set-up for PES on RGS is given (56). The role of the Seya Namioka is taken over by an energy analyzer for photoelectrons. PEY's, however, are not measured with the analyzer (because of intensity reasons) but with a copper grid in front of the sample. The copper grid is kept at a potential of +1 kV and electrons are measured independent of their kinetic energy (total yield in contrast to "partial" yield curves in luminescence). The set up of Fig. 13 also includes the possibility to measure the thickness of rare gas layers by interference patterns as well as reflectivity of the samples.

The discussion of the decay processes in RGS will be divided into three parts:

(1) Radiative decay.

(2) PLY and PEY curves in the excitonic region of excitation which contain information about energy transfer phenomena and motion of excitons.

(3) PLY and PEY curves at higher excitation energies. Here mainly electron-electron scattering will be discussed. EDC's play an important role in this context.

3.2 Radiative decay of excited states of rare gas solids

The first luminescence measurements on RGS have been published by Jortner et al [57] who used an α-source (^{210}Po) for excitation purposes. Since then, several investigations have been carried out using different excitation sources like high energy electrons (MeV region) [58,8,59-64], low energy electrons (~500 eV) [65-67], x-rays [70-75], α-particles [76-81] and finally VUV-light [82-88,55].

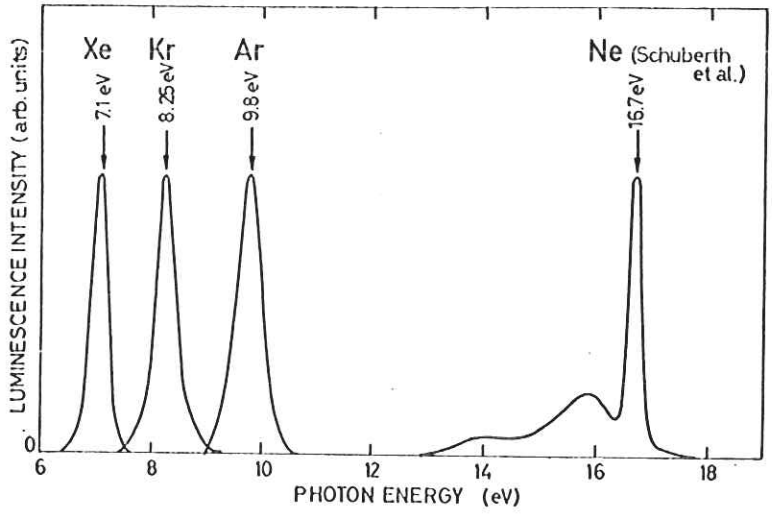

Fig. 14 Luminescence bands of RGS. The Xe, Kr, and Ar bands are taken from Ref. 89 (optical excitation, 5 K). The Ne spectrum is taken from Ref. 73 (X-ray excitation, 6 K).

In Fig. 14, a survey is given on the main luminescence bands which are found with all kinds of excitation. In the case of Ar, Kr and Xe, broad bands are found without fine structure (Ar: 9.8 eV, Kr: 8.25 eV, Xe: 7.1 eV). These bands are strongly shifted to lower energies compared with the onset of absorption (Stokes shift). The relevant parameters are given in Table 5. The Ne emission consists of one rather narrow band at 16.7 eV (close to the energy of the n = 1 exciton) and two broad bands at lower energy (16.1 eV and ~14 eV). A high resolution analysis of the narrow emission band [65,74] exhibits some fine structures. The broad RGS luminescence bands are the promising candidates for VUV lasers.

The results obtained by different groups do not agree in all details both for different and identical excitation. The differences seem to be explainable by different purification as well as preparation conditions. Moreover, depending on the kind of excitation, defects may be introduced which influence the luminescence spectra.

Table 5 Luminescence properties of RGS. The dominating bands (of Ar, Kr, Xe) (relaxed STE) were measured by several groups (e.g. Ref. 57, 62, 68, 75, 86). The half width is given in brackets. (All energies in eV)

	Ne	Ar	Kr	Xe
emission of the relaxed STE		9.8 (0.55)	8.25 (0.45)	7.1 (0.4)
emission of the unrelaxed STE	16.1 (73,62) 16.0 (64) 14.0 (64,73)	11.37 (68)		
"high temperature" band		11.1 (86)		7.6 (59,62, 79,89)

emission of "free" excitons

Ne 16.49; 16.64; 16.66; 16.74; 16.79; 16.80; 16.91; 17.01 (Ref. 62)
16.6; 16.7; 16.75; 16.9; 16.95 (Ref. 65)
16.65; 16.7; 16.8; 16.9 (Ref. 73)
16.7 (Ref. 64)

Ar 10.58; 10.74; 10.89; 10.99; 11.53; 11.56 (center 16.7); 11.61; 11.67 (Ref. 62)
11.58; 11.64 (Ref. 68)

Kr 9.92; 9.96; 10.02; 10.12; 10.13 (Ref. 62)

Xe 8.18; 8.24; 8.34; 8.36; 9.0; 9.2; 9.4 (Ref. 62)
8.18; 8.33 (Ref. 69)
8.2 (Ref. 81)

The striking features of RGS luminescence (Fig. 14) are:

(1) They are very similar to the emission bands of liquid and gaseous rare gases at higher pressures (500 Torr) (57). This is a striking behaviour compared to other kinds of solids.

(2) RGS luminescence bands have a very large Stokes shift.

(3) RGS luminescence bands have a large width and no fine structure (except of Ne).

Besides the luminescence bands shown in Fig. 14, under certain experimental conditions, some other bands show up, which are due to the pure RGS and not to impurities or defects:

(1) At elevated temperatures ($T \gtrsim 50$ K), solid Xe emits an additional broad band centered at ~7.6 eV [59,79,89]. A typical set of luminescence spectra at different temperatures is presented in Fig. 15. The branching ratio between both bands has a remarkable temperature dependence. For solid Ar, there is some indication that besides the 9.8 eV band a weak band at 11.1 eV [86] ($T \gtrsim 20$ K) and 11.37 eV [68] exists.

(2) Besides the broad luminescence bands very weak sharp luminescence lines are found for solid Ar [62,68], Kr [62] and Xe [62,69,81]. These lines are slightly Stokes shifted compared to n = 1 excitons. Obviously they are only found in well annealed samples. In Fig. 16, we present the Xe results as an example [69].

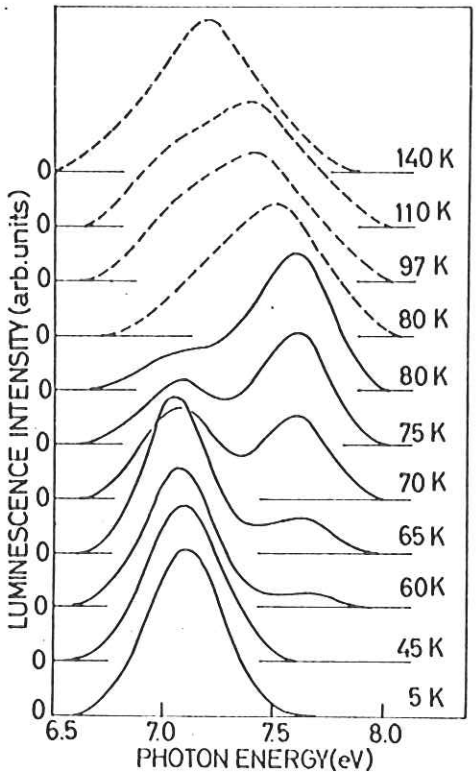

Fig. 15 Temperature dependence of the Xe luminescence bands excited by α-particles (resolution .2 eV) and VUV-light (dashed curves; resolution .4 eV) [89]

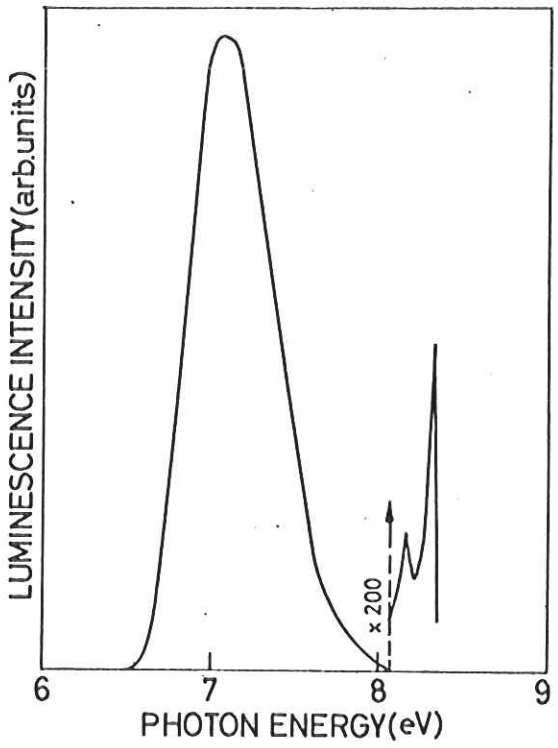

Fig. 16 Luminescence of solid Xe including the weak "free exciton" emission [69]

Another group of luminescence bands of RGS which mainly show up under e^--excitation should be mentioned. They are found between 7 eV and 4 eV for Ar, Kr and Xe [68,60,62]. In other investigations

they do not show up (e.g. under α-excitation and optical excitation) In Ref. 63 and 84 it was indicated that these bands may be due to impurities. Therefore they are no longer discussed here.

The explanation of the radiative decay mechanism in RGS starts from the close similarity of the luminescence bands in all three phases. From this similarity it was concluded that in the solid the decay mechanism should be similar to the decay mechanism of the gaseous phase. In gaseous rare gases, it has been shown by Tanaka (90) that an excited rare gas atom $R^*(^3P_{1,2})$ can form a covalently bound molecule together with a $R(^1S_o)$ ground state atom:

$$R^*(^3P_{1,2}) + R(^1S_o) \rightarrow R_2^*(^{1,3}\Sigma_u). \qquad (7)$$

The potential curves of such molecules in the gas phase have been discussed by Mulliken (91). A schematical configurational coordinate diagram is given in Fig. 17. The ground state of this molecule is strongly repulsive apart from a very shallow van der Waals minimum.

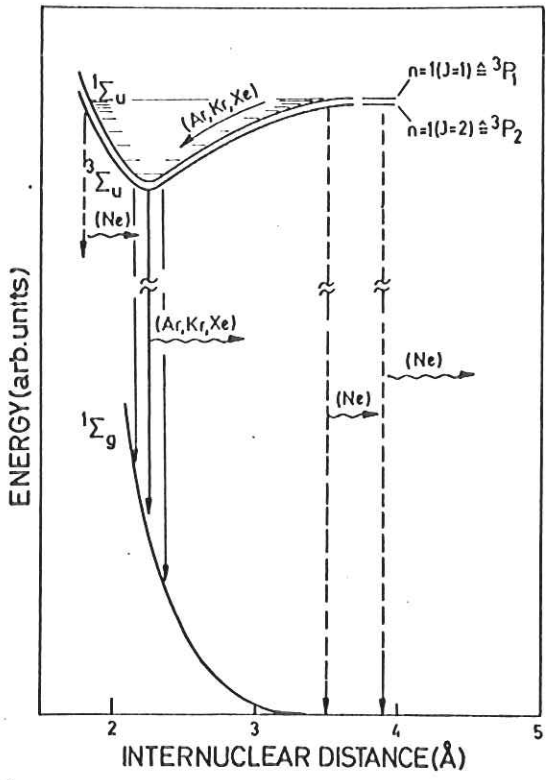

Fig. 17 Potential curves of a diatomic rare gas molecule (realistic for Ar_2). The vibrational relaxation process (Ar,Kr,Xe) and the explanations of the dominating luminescence bands are indicated by arrows.

Initially after formation the molecule is vibrationally excited. Via collisions with rare gas atoms it can relaxe to the vibrational ground state of the electronic excited state. The vibrational relaxation competes with the radiative decay of the molecule. At high pressures ($p \gtrsim 500$ Torr) the vibrational relaxation is much faster than the radiative decay of vibrational excited states. Therefore, only the radiative decay of the vibrationally relaxed

molecule can be measured (the so-called second continua of gaseous rare gases). At lower gas pressures, the vibrational relaxation is slowed down. In this case, luminescence is obtained from the vibrational excited molecules (the so-called first continua of gaseous rare gases). The large Stokes shift of rare gas luminescence is explained within this model by a) the depth of the potential curve of the excited state, and b) the height of the repulsive ground state potential curve at the internuclear distance at which the radiative decay takes place. The width of the broad luminescence bands directly reflects the steep slope of the repulsive ground state.

In the solid, we know (see Sec. 2.2) that the n = 1 excitons are located within - roughly speaking - one unit cell. They closely correspond to an atomic excitation ($n = 1 \hat{=} R^*(^3P_1)$). It is assumed that a slight spacial displacement of such an excited atom and a nearest neighbour in its ground state relative to each other leads to molecule formation within the solid. This process is called "self trapping" of the exciton, and the molecule itself "self trapped exciton" (STE). The formation of STE has been treated theoretically by Martin (92,93) and Molchanov (94).

The time τ_{ST} required for the self trapping process has been calculated by Martin (93) and is of the order of 5×10^{-12} sec. This is very fast compared to the radiative lifetime of a dipole allowed transition.
Similar to the gas phase, also in the solid the molecular center is formed in a highly vibrational excited state. Via coupling to the lattice, vibrational energy can be converted into phonons. Multiphonon processes are necessary because the vibrational quanta exceed the energy of phonons. In Ref. 11 an estimate for the order N of multiphonon processes is given. With increasing atomic weight, it decreases from $N \approx 18$ for Ne_2^* to $N \approx 3 - 6$ for the heavier rare gases. Therefore the vibrational relaxation is slow in solid Ne and fast in solid Ar, Kr and Xe.

The vibrationally relaxed STE is the lowest excited electronic state in RGS. It's radiative decay leads to the broad emission bands which are observed in solid Ar, Kr and Xe. They correspond to the second continua of the gas phase. In solid Ne, the relaxed STE is not reached. The vibrationally excited STE decays before a complete relaxation. Two luminescence bands can show up in this case corresponding to the two turning points of the vibrationally excited STE. In Ref. 73 the two broad luminescence bands at 16.1 eV and 14 eV are attributed to the radiative decay of the vibrationally excited STE at both turning points and thus correspond to the first continua of the gas phase. The different behaviour of Ne compared with Ar, Kr and Xe is indicated in Fig. 17. The weak 11.37 eV band of solid Ar (68) seems to be due to the decay of the vibrationally excited STE in analogy to the behaviour of solid Ne. For the "high temperature" bands (see Table 5) of solid Ar and solid Xe, an unambiguous explanation is still lacking.

From other solids like semiconductors it is known that free excitons contribute to luminescence. In RGS, the radiative decay of free excitons competes with the self trapping process. Because $\tau_{ST} \ll \tau_R$, in early measurements no radiative decay of free excitons was observed. The question whether there exist sharp luminescence lines due to the radiative decay of free excitons gained much theoretical interest. Toyozawa (95) pointed out, that the free exciton state in RGS should be metastable with respect to exciton-lattice interaction and not unstable. In other words, the free exciton and the STE should be separated by a potential barrier. As a consequence, sharp emission lines of the free excitons should show up in RGS. This was proved recently by different groups (see Table 5). From the branching ratio between the emission of the vibrationally relaxed STE and the free exciton, the self trapping time for Xe excitons could be estimated (81). The experimental value of $\tau_{ST} \approx 2 \times 10^{-11}$ sec is slightly longer than the value calculated by Martin (93). The sharp emission lines (see e.g.Fig. 16) are slightly Stokes shifted (some tenths of an eV). The Stokes shift is explained by a cubic relaxation of the lattice around the free exciton.

In solid Ne, the main emission band at 16.7 eV is explained by the radiative decay of free excitons after the cubic relaxation. The potential barrier between the free state and the STE seems to be so high that $\tau_R \lesssim \tau_{ST}$.

Measurements of radiative lifetimes of the STE as well as of the free excitons in RGS have not been published up to now. Such measurements would give detailed information on the molecular states of the STE which split in the crystal field of the solid (94). Lifetime measurements on RGS are performed now with pulsed electron excitation by Hahn et al (96). Preliminary results on solid Xe indicate two components of the STE luminescence: a fast one of some ns and a slow one, the decay time of which varies between ~150 ns and ~1 µs depending on temperature (96). The time characteristics of solid Xe luminescence seem to be similar to the behaviour of the gaseous phase at high pressures (97) concerning the appearance of a slow and a fast decay time. But the long decay time exceeds the gas value by an order of magnitude at low temperatures.

3.3 Photoluminescence and photoelectric yield of rare gas solids in the excitonic region of excitation

In the previous section we have discussed steps 3 and 4 of the decay processes outlined in Fig. 11. Now we proceed with step 2. Step 2 includes (1) relaxation of higher members of the exciton series to the n = 1 exciton, (2) motion of free excitons, (3) energy transfer in doped samples from the host excitons to guests. It turns out that all these processes show up in the yield curves of the two decay channels photoluminescence and photoelectron emission.

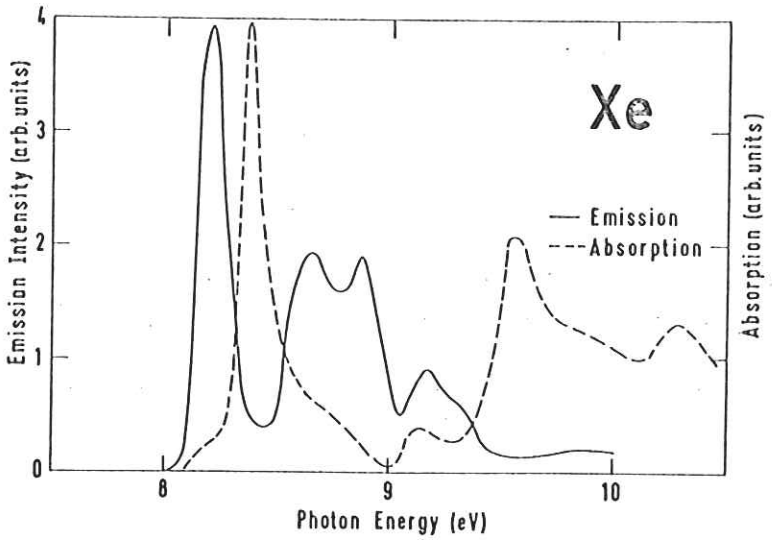

Fig. 18 Photoluminescence yield of the 7.1 eV band of solid Xe (86). The dashed curve is an absorption spectrum of solid Xe (20). The luminescence intensity is normalized to the incident intensity of the exciting light.

The first photoluminescence yields (PLY) of RGS luminescence bands were measured by Nanba et al (83) (7.1 eV band of Xe) and Brodmann et al (85,86) (7.1 eV band of Xe, 8.25 eV band of Kr and 9.8 eV band of Ar) with the set up of Fig. 12. In Fig. 18 the result on solid Xe of these early measurements is shown (86) together with an absorption curve of solid Xe (20). The main features of the PLY are pronounced maxima at the low and high energy side of the excitons (especially of the n = 1 $\Gamma(3/2)$ exciton) and deep minima at the energy of the excitons themselves. This indicated a low luminescence efficiency for excitation at the energy of absorption maxima and a high luminescence efficiency for excitation of the tails of absorption maxima. This behaviour was not understood at all at the beginning of these investigations.

It was argued, however, that perhaps surface effects could play an important role (86). Improving the vacuum in the sample chamber to $\sim 10^{-9}$ Torr made it possible to investigate the influence of surface effects (55,87). It turned out, that even a fraction of a monolayer of contamination is able to quench the luminescence. This is demonstrated in the left part of Fig. 19 which shows a set of PLY curves of the Kr 8.25 eV luminescence band. Curve I has been obtained from a sample immediately after preparation. The minima in this curve at 10.2 eV, 10.85 eV and 11.22 eV coincide with the energies of the n = 1 $\Gamma(3/2)$, n' = 1 $\Gamma(1/2)$ and n = 2 $\Gamma(3/2)$ excitons. Curves II to V are obtained from the same sample with increasing surface contamination. The minima get more and more pronounced until nearly static curves are obtained (curve V).

This behaviour is explained by an energy transfer from excitons to the contaminant at the surface. Because the acceptors for the

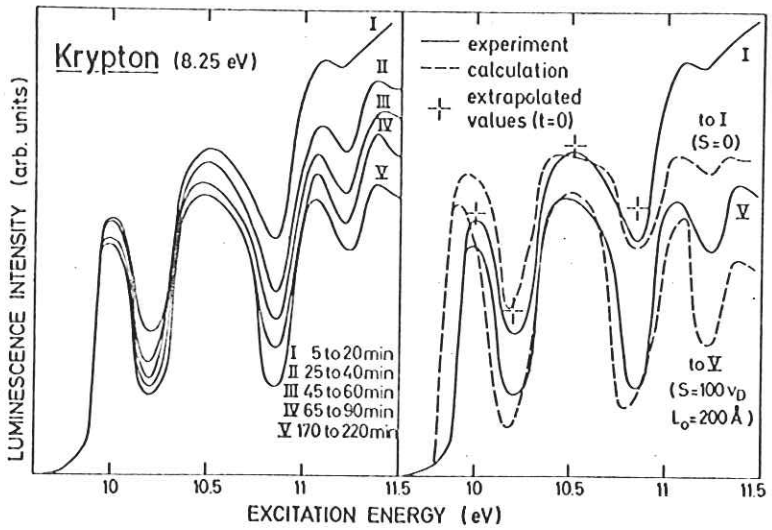

Fig. 19 Time dependence of the PLY curves of the 8.25 eV Kr luminescence band due to increasing contamination. Experimental results on the left. Comparison with model calculations on the right.

energy transfer are in a geometrically well defined position of the samples, their influence on the PLY can be calculated quantitatively. However, assumptions must be made on the kind of energy transfer which takes place (55).

In the case of PLY spectra of RGS, two different models for the energy transfer have been applied (55,87)

(1) Diffusive motion of free excitons and "collision induced" energy transfer to the acceptor atoms at the surface.

(2) Energy transfer from immobile excitons (STE) to the acceptor atoms at the surface by dipole - dipole interaction according to Förster's theory (98).

In the "diffusion model" the starting point is the fact that the PLY is proportional to the steady state number of STE which itself is proportional to the steady state number of free excitons, N. Under normal incidence conditions, N is given by

$$N \sim \int_0^d n(x)dx \qquad (8)$$

where x means the coordinate perpendicular to the surface and d means the thickness of the sample. n(x) is the steady state concentration of free excitons.
n(x) is calculated from a diffusion equation

$$D \cdot \frac{d^2n}{dx^2} = \frac{n}{ST} - J_o \cdot \alpha \cdot \exp(-\alpha x) \qquad (9)$$

containing a diffusion term (D: diffusion coefficient of free excitons), a decay term for free excitons (τ_{ST}: self trapping life time; the radiative lifetime being neglected) and a generation term (J_o: intensity of incident light, α: absorption coefficient). The influence of energy transfer from excitons to the acceptor atoms is introduced by the boundary conditions

$$-D\cdot\left(\frac{dn}{dx}\right)_{x=o} = -n(0)\cdot s;\quad D\left(\frac{dn}{dx}\right)_{x=d} = -n(d)\cdot s^{*} \qquad (10)$$

(s, s^{*}: surface recombination velocity at the front and the back, respectively).

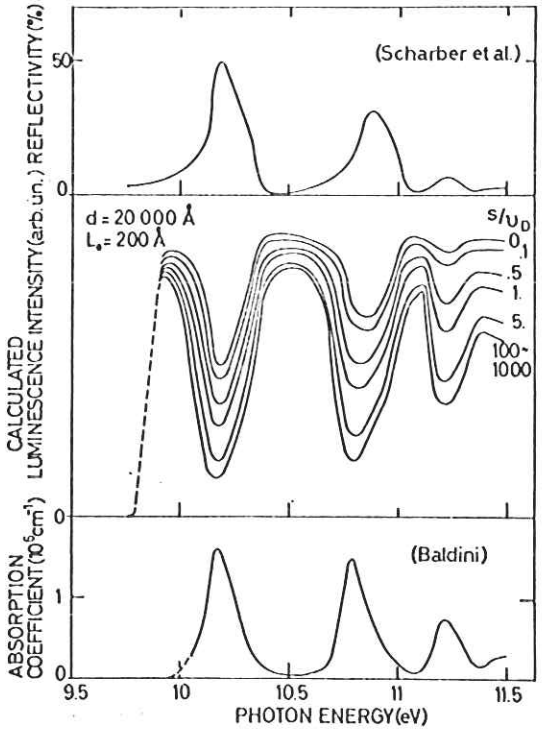

Fig. 20 PLY's of the 8.25 eV Kr band obtained from the diffusion model (in the middle), together with the input data (reflectivity from Ref. 20, absorption from Ref. 12)

The dependence of N on the excitation energy is introduced by the energy dependence of the absorption coefficient. The solution for the PLY curve contains two unknown quantities: the diffusion length $L_o = \sqrt{D\cdot\tau_{ST}}$ of free excitons and the ratio s/v_D where v_D means the diffusion velocity $v_D = L_o/\tau_{ST}$. s^{*} does not show up in the solution, if $d \gg \frac{1}{\alpha}$. In Fig. 20 a set of calculated PLYs is given for different values of s/v_D, together with the input data of the absorption coefficient α (12) and reflectivity R(20). $s/v_D = 0$ means no energy transfer at the surface (no acceptor atoms being present), $s \gg v_D$ means $n(0) \approx 0$, all free excitons reaching the surface transfer their energy to acceptor atoms. With $s = 0$ a fairly good fit of the PLY of the nearly clean sample is possible. This is demonstrated in Fig. 19 (upper two curves in the right part). The energy dependence of the PLY in the excitonic region of ex-

citation is exclusively introduced by the reflectivity of the sample (PLY is normalized to the incident intensity). With $s \gg v_D$ and a diffusion length of 200 Å a fairly good fit of the PLY V of Fig. 19 is possible (see right part of Fig. 19, lower curves). Ackermann et al [55,87] conclude:

(1) The diffusion length of free excitons in solid Kr is ~200 Å, provided, excitons do move.

(2) The spectra can be explained by approximately the same diffusion length for the n' = 1 as well as for the n = 1 exciton.

The latter point perhaps indicates an electronic relaxation of higher excitons to the n = 1 exciton which is much faster than self trapping ($\tau_{Rel} \ll \tau_{ST}$). In this case only the dynamics of the n = 1 exciton show up in the PLY.

The dipole - dipole transfer model is also able to explain the PLY. In this model, the interaction strength between immobile excitons and the acceptor is characterized by a critical radius R_o [98]. For the geometry used in the experiment it is more convenient to characterize the energy transfer to the surface by a length, d_o, given by

$$d_o^4 = \frac{\pi}{2} R_o^6 \cdot n_a \qquad (11)$$

where n_a means the number of acceptors/cm^2 at the surface. d_o can be regarded as the thickness of a "dead layer" for excitons near the surface. Fig. 21 shows a comparison of a calculated PLY and the measured PLY V of Fig. 19. From d_o = 80 Å, a value of $R_o \approx 22$ Å is obtained. This value is in good agreement with R_o = 17 Å calculated according to Förster's theory [98].

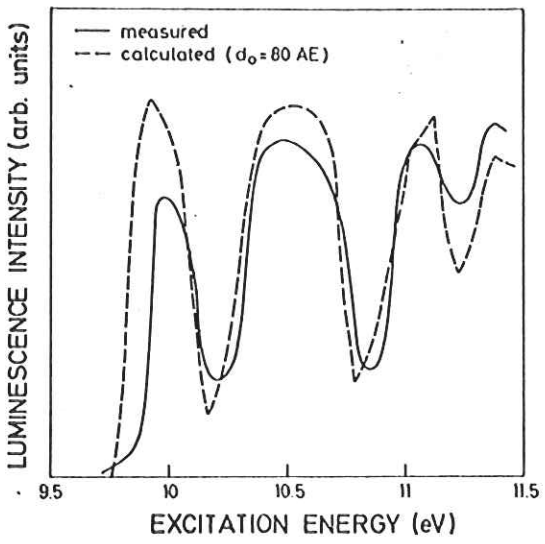

Fig. 21 Comparison between the measured PLY of the 8.25 eV Kr band (curve V of Fig. 19) and a model calculation (dipole-dipole energy transfer model).

At the present time, from point of view of PLY spectroscopy, it is not clear whether diffusive motion of free excitons or dipole - dipole interaction between immobile (STE) excitons and acceptor atoms is the dominating contribution to energy transfer processes.

Recently, the PLY of both the host and guest luminescence of C_6H_6 doped RGS has been measured as a function of impurity concentration (99). The ratio of the luminescence intensities not only depends on the concentration but also on the excitation energy. It was concluded that a complicated balance between both energy transfer processes has to be taken into account in this special system.

As an excellent tool for the investigation of electronic relaxation processes and of the dynamics of free excitons in RGS, PEY-measurements can be used.

Since the early work of O'Brien et al (100) who investigated the PEY of solid Kr and Xe for excitation energies below the LiF cutoff it is known that photoemission not only occurs above the threshold given by the vacuum level but also below the intrinsic threshold. This kind of photoemission was explained by exciton-impurity interaction. The mechanism of this impurity enhanced photoemission is explained in Fig. 22. It shows an energy scheme of a RGS with the

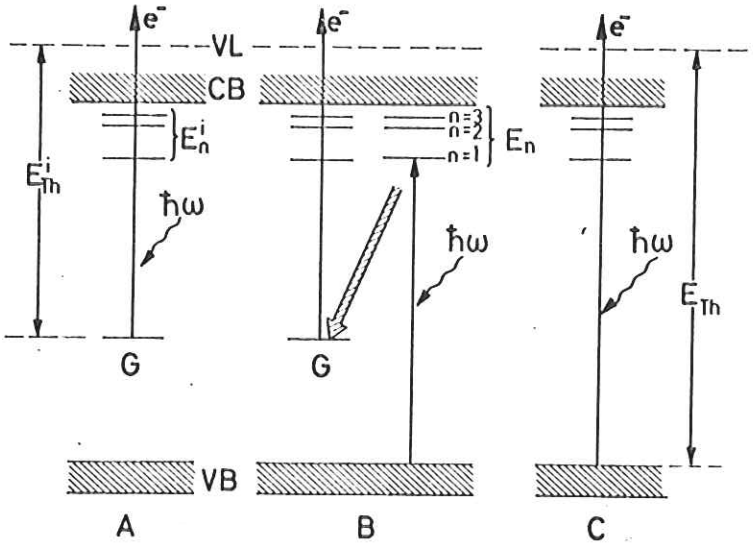

Fig. 22 Models for the photoemission mechanisms in pure and doped RGS.

valence band, VB, the conduction band, CB, the host exciton levels n = 1,2... and impurity exciton levels E_n^i. E_{TH} represents the energetical position of the vacuum level. If a host exciton transfers its energy E_n to the guest G, the latter may be ionized. Depending on the depth of the impurity level and the position of E_{TH}, the free electron can have an energy above or below E_{TH}. If its energy is above E_{TH}, photoemission shows up. In a series of papers (101-106), impurity enhanced photoemission of RGS was investigated consciously in order to study exciton dynamics and energy transfer phenomena.

Two methods have been applied:

(1) Detection of photoelectrons resulting from the decay of free excitons at the interface sample-vacuum or sample-substrate in pure RGS (102,105,107) (extrinsic photoemission).

(2) Detection of photoelectrons resulting from impurity ionization in doped RGS (101,103,104,106,107).

In the first group of experiments, for the interaction between excitons and the substrate (Au) two mechanisms have been considered:

(1) Förster - type dipole - dipole interaction between STE and the Au substrate.

(2) Diffusion of free excitons and "collision induced" energy transfer to the substrate.

The key experiment in order to distinguish between both energy transfer processes was the dependence of PEY curves on the thickness of the layers. Förster - type energy transfer was ruled out from the results. In the framework of exciton diffusion, the steady state concentration of free excitons, $n(x)$, was calculated from a diffusion equation similar to Eq.(9) under the assumption of the following boundary conditions: $n(0) = 0$, $n(d) = 0$, d being the thickness of the layer. From $n(x)$, the flux of free excitons through the interface $(-D \cdot dn/dx)_{x=d}$ was calculated. The number of photoelectrons leaving the substrate is proportional to the exciton flux. Multiplication of the flux with $\exp(-d/l)$, l being the attenuation length of photoelectrons in the sample results in the exciton enhanced PEY. From fits of the experimental data (dependence of PEY on thickness as well as excitation energy) values are obtained for the diffusion lengths of free excitons as well as attenuation lengths for photoelectrons in RGS are obtained. The results are summarized in Table 6 together with exciton diffusion lengths extracted from PLY curves.

Table 6 Diffusion lengths (L_o) of free excitons and attenuation lengths (l) of photoelectrons in RGS

	Ne	Ar	Kr	Xe	Method
L_o (Å)	2500 (107)	120 (105)		75 (101) 150 (104)	exciton enhanced impurity photoemission
L_o (Å)	>4000 (107)			300 (104)	extrinsic photoemission
L_o (Å) ($T^o < 10K$)		50 (87)	200 (55)	150 (87)	PLY curves
l (Å)	3500 (107)	1200 (105)		850 (104)	extrinsic photoemission

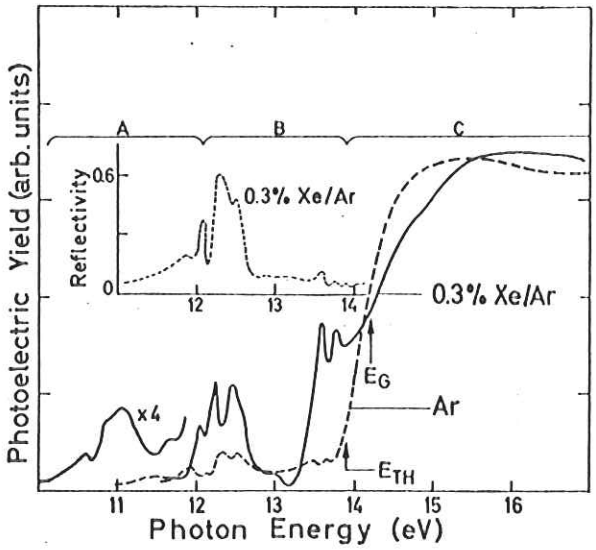

Fig. 23 Photoelectric yield per photon penetrating the sample for 0.3% Xe in Ar (solid curve) and pure Ar. The insert shows the reflectance measured simultaneously.

In the second group of photoemission experiments, the PEY of doped RGS is measured. In Fig. 23 a typical result is presented (.3% Xe in Ar) (105). Three energy regions in the PEY must be considered. In region A, impurities are directly excited above the impurity threshold. In region B, exciton states of the host are excited. In this case, energy transfer from the host exciton states to the impurity states leads to photoemission. In region C, direct photoemission from the host matrix at energies above the matrix threshold is observed. The processes A, B, C are elucidated in Fig. 22. A comparison between the PEY of the Xe doped sample (full curve) and of undoped Ar (dashed curve) clearly shows an enhancement of the PEY by doping. The line shape of the PEY in region B sensitively depends on thickness. In very thin layers ($d \approx 90$ Å) the PEY shows maxima which coincide with the absorption maxima of the matrix. With increasing thickness, the PEY shows dips corresponding to the absorption maxima of the matrix. These dips are similar to the minima in the PLY curves of samples with a surface layer of acceptors. The shape of the PEY in region B contains information about the kind of energy transfer from the host exciton states to the impurities. Only free excitons have to be considered because the energy available from the STE is smaller than the impurity threshold energy. The PEY is given by

$$Y = \frac{S\,[R]}{J_o} \int_o^d \exp(-x/l) \cdot n(x)\,dx \qquad (12)$$

where $n(x)$ is the steady state concentration of free excitons, l the attenuation length of photoelectrons, d the sample thickness, $[R]$ the concentration of impurities, S the rate constant for impurity ionization and J_o the incident light intensity. $n(x)$ is governed by a diffusion equation similar to Eq.(9) which must be completed by an energy transfer term $-S \cdot [R] \cdot n(x)$ (steady state conditions). The model calculations for the PEY according to Eq. 12

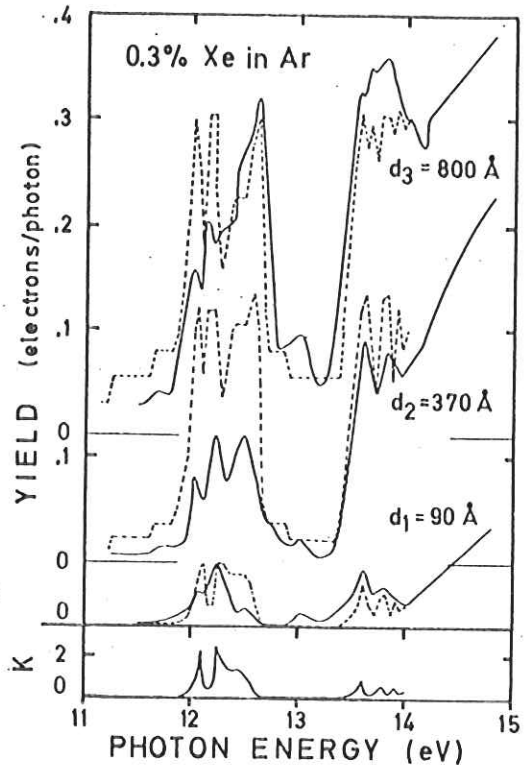

Fig. 24 Comparison of calculated and measured PEY's for 0.3% Xe in Ar for three film thicknesses.

with n(x) obtained from the diffusion model fit the experimental results quite well if the boundary conditions $n(0) = 0, n(d) = 0$ are used. This is shown in Fig. 24 where PEY curves of three samples with different thicknesses are compared with the model calculations.

Not only the yield itself but also its dependence on the impurity concentration was measured and compared with the model calculations. From the fits of the measurements by the model calculations the following quantities are obtained: the diffusion length of free excitons and $S \cdot \tau_o$ (τ_o: lifetime of free excitons). The results for solid Ne, Ar, Kr, and Xe are summarized in Table 6. Good agreement between the values for the diffusion lengths obtained by luminescence and photoemission measurements is found.

From the PEY curves of exciton enhanced impurity photoemission it cannot be decided from which host state the energy transfer takes place if a higher exciton is excited. Such informations are obtained from EDC's.

In the case of Xe doped Ne and Xe doped Ar such measurements have been carried out for the first time by Schwentner and Koch (56). They found striking differences between both systems. In Xe doped Ne, the internal relaxation from higher members of the exciton series to the n = 1 exciton is so fast, that in the EDC's of the exciton enhanced impurity photoemission only a transfer of the energy of n = 1 excitons can be found. In Xe doped Ar, however, also unrelaxed n = 2 excitons show up in the EDC's. From this kind of measurements it was possible to obtain time hierarchies for the various competing decay processes in these systems.

3.4 Photoluminescence - and photoemission yield curves for higher excitation energies

In this chapter we want to discuss the yield spectra for excitation energies up to ~50 eV. In this energy range where the initial excitation process results in a hole and an electron with high kinetic energy, the processes summarized as step 1 of the crude decay model of Fig. 11 show up. These are mainly electron - phonon scattering, electron - electron scattering and in doped samples electron-impurity scattering. Electron-phonon scattering in solid rare gases is rather inefficient because of lack of optical phonons and because the acoustical phonons have very small energies (108). Therefore electron-electron scattering will be in the foreground of discussion.

The nature of scattered states can be concluded from the yield curves of both kinds of measurements. The scattering probability can be obtained from an energy analysis of the photoelectrons. It also shows up in PLY's. A quantitative deduction of scattering probabilities from PLY's of RGS, however, is not available up to now.

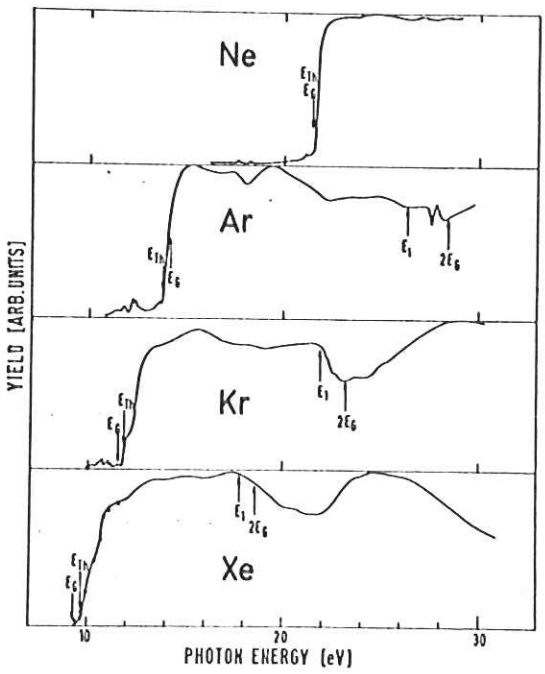

Fig. 25 Photoemission yield curves of solid Ne, Ar, Kr, and Xe.

In Fig. 25, the PEY curves of RGS are shown for excitation energies up to 30 eV (52). Above threshold, E_{TH}, the PEY is nearly independent of excitation energy until the energy $E_1 = E_g + E_{ex}$ (E_{ex}: energy of the n = 1 exciton) is reached. Above E_1^g, the PEY of solid Kr and Xe show a marked decrease. This decrease is not present in the curve of solid Ar. The energy E_1 is interpreted as the onset of electron-electron scattering (52,109). It is assumed that at the onset the initially excited photoelectron is scattered

to the bottom of the conduction band and an exciton (n = 1) is produced. In the case of solid Kr and Xe, both scattered states are below the threshold energy E_{TH} for photoemission. Therefore electron-electron scattering leads to a decrease of the PEY around the onset. In the case of solid Ar, the vacuum level is below the bottom of the conduction band. The scattered photoelectron still contributes to photoemission and the PEY is not influenced by electron-electron scattering at the onset. (The vacuum levels of RGS are indicated in Fig. 10 as E_V). With increasing excitation energy, $\hbar\omega > 2E_V$ the PEY's of solid Kr and Xe increase again. This indicates that now at least one of the scattered states has an energy above the vacuum level.

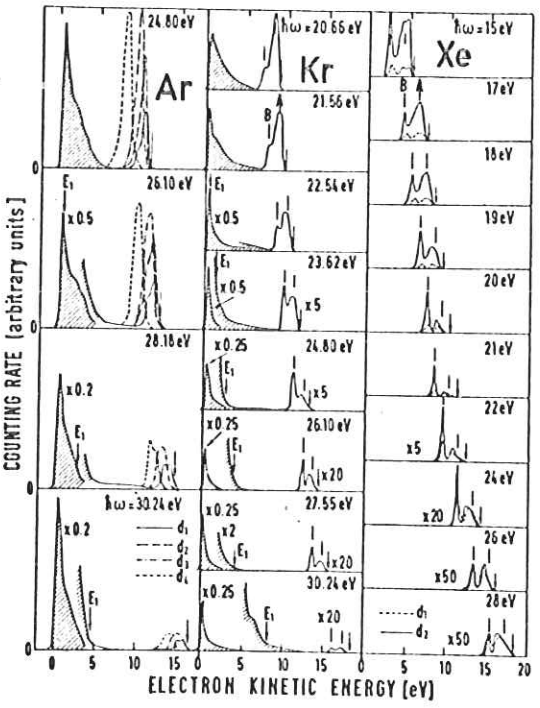

Fig. 26 EDC's of solid Ar, Kr, and Xe in the region of electron-electron scattering. Explanations are given in the text.

Much deeper insight into electron-electron scattering is obtained from EDC's as presented in Fig. 26 [110]. The excitation energies indicated in the Figure have been chosen from the region slightly below and above $2E_g$. The unshadded parts of the EDC's show the energy distribution of photoelectrons which have not been scattered whereas the shadded curves show the energy distribution of scattered electrons. The maxima A, B contain information about the density of states of the valence bands (see Sec. 2.8). With increasing excitation energy the ratio A/B is drastically changed because the scattering onset for photoelectrons from the upper valence band ($\sim$ maximum A) has a lower energy than the scattering onset for photoelectrons from the lower valence band ($\sim$ maximum B). In the case of Ar and Xe, in Fig. 26 results from samples with different thickness are included. Schwentner [110] deduced the energy dependence of the mean free path L(E) from both the decrease of the number of unscattered electrons associated with a

distinct initial energy when the electron kinetic energy is varied through $\hbar\omega$ and also from the thickness dependence of the number of unscattered electrons. In Fig. 27, L(E) is shown as a function of electron energy measured from the top of the valence band. For excitation energies below $E_1 = E_g + E_{ex}$, the scattering lengths exceed

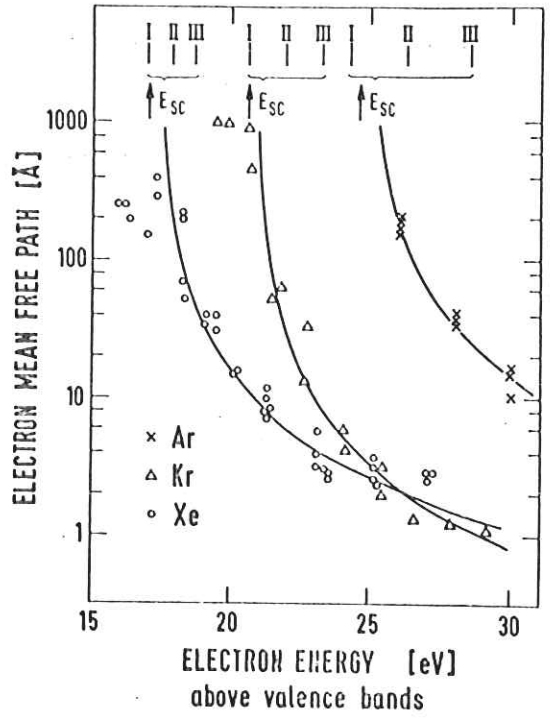

Fig. 26 Mean free path of photoelectrons in the region of electron-electron scattering for solid Ar, Kr, and Xe.

~1000 Å. The energy E_1 is included in Fig. 27 with "II". With increasing energy of the photoelectrons, the scattering length is drastically reduced to values around 1 - 5 Å in the case of Kr and Xe and to ~10 Å for Ar (for Ar perhaps the minimum cannot be reached within the range of electron energy covered by the experiment). The small scattering lengths are found for electron energies slightly above 2 x E_g (indicated by "III"). The curves in Fig. 27 are the results of a model calculation [110] for L(E). This calculation gives information about the onset of electron-electron scattering, E_{SC}, which is included in Fig. 27 by arrows. In the case of solid Kr and Xe, E_{SC} is very close to twice the energy of the n = 1 excitons, indicated by "I".

These results are very surprising. They indicate that at the onset both scattered states are excitons. In the case of solid Ar, the onset energy E_{SC} corresponds more to E_1 indicating that the scattering process at the onset is governed by the production of one exciton and one electron-hole pair. These results will be discussed below in connection with similar luminescence results.

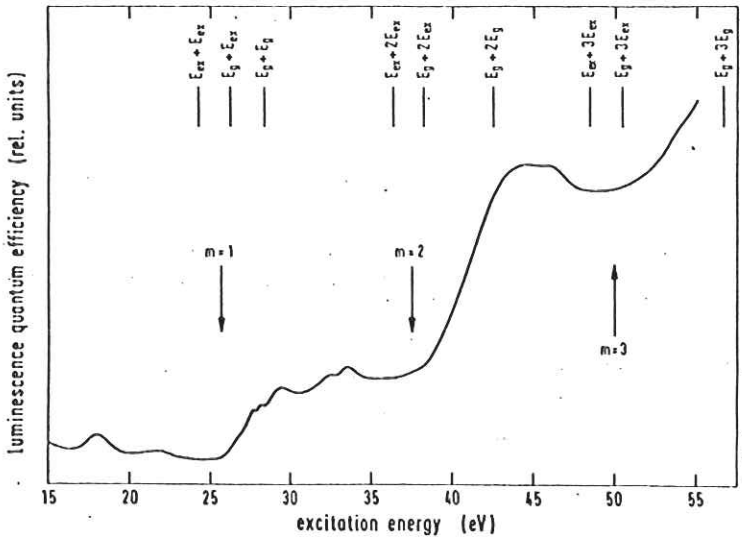

Fig. 28 PLY of the 9.8 eV luminescence band of solid Ar.

Photoluminescence yield curves for higher excitation energies have been published up to now only in the case of solid Ar [88]. In Fig. 28, the PLY curve (luminescence quantum efficiency in relative units) of the intrinsic Ar luminescence band at 9.8 eV is presented. The most exciting feature of this curve is the stepwise increase with increasing excitation energy. The onset energies for these steps are indicated by arrows (m = 1,2,3). They closely correspond to the energies $E_g + m \cdot E_{ex}$ which are the expected onsets for the production of one electron-hole pair and m excitons (n = 1) via electron scattering of the initially excited state. In contrast to photoemission, in luminescence all the scattered states show up in the radiative decay channel which explains the steps of Fig. 28. The step m = 1 has been discussed in more detail [88]. In Fig. 29 the PLY is compared with the scattering length of photoelectrons in solid Ar, taken from Fig. 27. The energetic position of the luminescence increase and the decrease of the scattering length (indicating an increase of the scattering probability) are in excellent agreement. It was pointed out [88] that the three step model underlying a temporary description of electron-electron scattering ((1) initial excitation, (2) motion of the photoelectron, (3) scattering process) might be problematic for scattering processes characterized by a scattering length smaller than the nearest neighbour distance of the solid. Therefore, in Ref. 88, it was proposed that perhaps the process of excitation itself produces the scattered states in the framework of "electronic polaron complex" excitation, discussed by Devreese et al [111] for alkali halides. An excited state of the "electronic polaron complex" consists of an electron and a hole, both surrounded ("dressed") by an electronic polarization cloud, and an additional exciton. This exciton is a real quantum of the (exciton) boson field which couples to excess

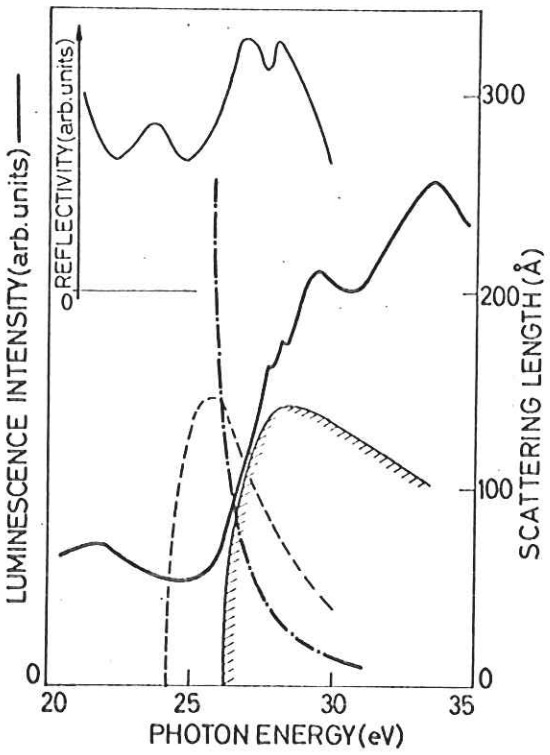

Fig. 29 Comparison between the PLY of the 9.8 eV Ar luminescence band and the scattering length for photoelectrons for excitation energies around 2 E_g. The estimated cross sections for the bound (----) and free (77777) electronic polaron complex and the reflection curve of solid Ar around 2 E_g are included.

charges in insulators forming the electronic polaron (111). Two different types of electronic polaron complexes are possible: in the bound complex, the dressed electron is coupled to the dressed hole via Coulomb interaction; in the free complex, this Coulomb interaction is neglected.

In Fig. 29, the expected cross sections for electronic polaron complex excitation are sketched in analogy to the curves presented for alkali halides (111). Whereas the bound complex does not show up significantly in the PLY the increase of luminescence around $E_1 = E_g + E_{ex}$ nicely corresponds to the cross section of the free complex. The question arises whether such an excitation also shows up in absorption. Because no direct absorption measurements on solid Ar are available for photonenergies around 2 E_g we analyzed reflection measurements on solid Ar in this energy range (109). Indeed, there shows up a pronounced structure in reflection which could correspond to the free complex.

PLY measurements perhaps are not conclusive enough to establish the creation of excited electronic polaron complexes. However, the onset energies E_{SC} for electron-electron scattering in photoemission of solid Kr and Xe also point to the creation of electronic polaron complexes. E_{SC} of solid Kr and Xe closely corresponds to $2 \cdot E_{ex}$. This onset can hardly be understood in a temporary model. It could be easily understood in the framework of the bound electronic polaron complex.

As already mentioned, inelastic electron-phonon scattering is rather inefficient in RGS. The situation can change drastically when the fcc structure of RGS is changed to hcp. Then optical phonons are present which amplify inelastic electron-phonon scattering. Such a phase transition leading to a mixture of fcc and hcp has recently been found in solid Ne at 10.5 K by Schuberth et al (74,112) with aid of luminescence spectroscopy. At 10.5 K, the γ-induced luminescence of solid Ne increases by nearly an order of magnitude compared to lower temperatures. This effect is due to a drastic reduction of competing non radiative processes because in the new phase slowing down of photoelectrons is accelerated by inelastic electron-phonon scattering. The interpretation of the measurements with a partial fcc→hcp phase transition was proved by the same authors by measuring Raman scattering below and above 10.5 K. Above 10.5 K a Raman active optical phonon clearly showed up whereas it was absent below 10.5 K.

Acknowledgements

The author is grateful to Professor R. Haensel who encouraged him in writing this article and who contributed very much with helpful discussions and comments. The critical reading of the manuscript by Dr. E.E. Koch and Dr. N. Schwentner, and helpful comments of H.W. Wolff are gratefully acknowledged. Special thanks go to R. Lohmann for the careful typing of the manuscript.

References

(1) Handbook of Chemistry and Physics, 52nd Edition (1971-1972) CRC, Cleveland

(2) C. Kittel, Introduction to Solid State Physics, 3rd edition, Wiley & Sons, New York (1966)

(3) Charlotte E. Moore, Circ. of the NBS 467, vol.I (1949); vol.II (1952), vol.III (1958)

(4) K.F. Niebel and J.A. Venables, in Rare Gas Solids, vol.I, ed. by M.L. Klein and J.A. Venables, Academic Press, London - New York - San Francisco (1976), p.558

(5) B. Sonntag, in Rare Gas Solids, vol.II, ed. by M.L. Klein and J.A. Venables, Academic Press, London - New York - San Francisco (1976, in press)

(6) U. Rössler, in Rare Gas Solids, vol.I, ed. by M.L. Klein and J.A. Venables, Academic Press, London - New York - San Francisco (1976), p.505

(7) R. Haensel, G. Keitel, P. Schreiber, and C. Kunz, Phys. Rev. Letters 22, 398 (1969)

(8) N.G. Basov, V.A. Danilychev, Yu.M. Popov, and D.D. Khadkevich, J.exp.theor.Phys. SSSR 10, 473 (1970)

(9) D.J. Bradley, in Lasers in Physical Chemistry and Biophysics, Elsevier Scientific Publishing Company, Amsterdam (1975), p.7

(10) Charles K. Rhodes, JEEE J. Quantum Electr. QE-10, 153 (1974)

(11) J. Jortner, in Vacuum Ultraviolet Radiation Physics, ed. by E.E. Koch, R. Haensel, and C. Kunz, Pergamon-Vieweg, Braunschweig, p.263 (1974)

(12) G. Baldini, Phys.Rev. 128, 1562 (1962)

(13) R. Haensel, in Festkörperprobleme (Advances in Solid State Physics), vol.XV, ed. by H.J. Queisser, Pergamon/Vieweg, Braunschweig, p.203 (1975)

(14) C. Kunz, Comments on Solid State Physics 5, 31 (1973)

(15) J.R. Nelson and P.L. Hartmann, Bull.Am.Soc. 4, 371 (1959)

(16) O. Schnepp and K. Dressler, J.Chem.Phys. 33, 49 (1960)

(17) D. Pudewill, F.-J. Himpsel, V. Saile, N. Schwentner, M. Skibowski, and E.E. Koch, phys.stat.sol. (b) 74, 485 (1976)

(18) V. Saile, Kramers-Kronig analysis of the data given in A. Harmsen, Diploma work, Hamburg (1975) and Int.Report DESY F 41 - 75/06 (1975)

(19) R. Haensel, E.E. Koch, U. Nielsen, and M. Skibowski, III. Intern.Conference on Vacuum Ultraviolet Radiation Physics, Tokyo (1971)

(20) J.T. Steinberger, J.Appl.Opt. 12, 614 (1973); evaluation of data of S.R. Scharber, Jr. and S.E. Webber, J.Chem.Phys. 55, 3985 (1971)

(21) Y. Onodera and Y. Toyozawa, J.Phys.Soc.Japan 22, 1410 (1967)

(22) V. Saile, thesis, München (1976)

(23) U. Rössler, phys.stat.sol. (b) 42, 345 (1970)

(24) W.B. Fowler, Phys.Rev. 132, 1591 (1963)

(25) M.H. Reilly, J.Phys.Chem.Solids 28, 2067 (1967)

(26) A.B. Kunz and D.J. Mickish, Phys.Rev. B8, 779 (1973)

(27) W. Andreoni, M. Altarelli, and F. Bassani, Phys.Rev. B11, 2352 (1975)

(28) G. Baldini, Phys.Rev. 137, A508 (1965)

(29) J.T. Steinberger, C. Atluri, and O. Schnepp, J.Chem.Phys. 52, 2723 (1970)

(30) A. Harmsen, E.E. Koch, V. Saile, N. Schwentner, and M. Skibowski, in Vacuum Ultraviolet Radiation Physics, ed. by E.E. Koch, R. Haensel, and C. Kunz, Pergamon-Vieweg, Braunschweig, p.339 (1974)

(31) V. Saile, M. Skibowski, W. Steinmann, P. Gürtler, E.E. Koch, and A. Kozevnikov, Phys.Rev. Letters 37, 305 (1976)

(32) A. Otto, in Festkörperprobleme XIV (Advances in Solid State Physics), ed. by H.J. Queisser, Pergamon-Vieweg, Braunschweig (1974), p.1
A. Otto, in Optical Properties of Solids, New Developments, ed. by B.O. Seraphin, North-Holland, Amsterdam (1976), p.677

(33) H.W. Wolff, private communication; to be published

(34) R.A. Tilton and C.P. Flynn, Phys.Rev. Letters 34, 20 (1975)

(35) R.A. Tilton and C.P. Flynn, to be published

(36) Y. Tanaka and K. Yoshino, J.Chem.Phys. 53, 2012 (1970); J.Chem.Phys. 59, 5160 (1973)
D.E. Freeman, K. Yoshino, and Y. Tanaka, J.Chem.Phys. 61, 4880 (1974)
M.C. Castex, Chem. Physics 5, 448 (1974)

(37) R. Brodmann and G. Zimmerer, to be published

(38) U. Rössler and O. Schütz, phys.stat.sol. (b) 56, 483 (1973)

(39) J.-Y. Roncin and K. Moorjani, phys.stat.sol. 23, K1 (1967)

(40) D. Beaglehole, Phys.Rev. Letters 15, 551 (1965)

(41) J.C. Phillips, Phys.Rev. 136, 1714 (1964)

(42) R. Haensel, G. Keitel, C. Kunz, and P. Schreiber, Phys.Rev. Letters 25, 208 (1970)

(43) R. Haensel, G. Keitel, P. Schreiber, and C. Kunz, Phys.Rev. 188, 1375 (1969)

(44) R. Haensel, G. Keitel, E.E. Koch, M. Skibowski, and P. Schreiber Opt.Commun. 2, 59 (1970)

(45) J.A.R. Samson, J.Opt.Soc.Am. 54, 842 (1964)

(46) R.B. Cairns, H. Harrison, and R.J. Schoen, Phil.Trans.Roy.Soc. A268, 163 (1970)

(47) D.L. Ederer, Phys.Rev.Letters 13, 760 (1964)

(48) A.P. Lukirskii and T.M. Zimkina, Opt.Spectroscopy 17, 234 (1964)

(49) R. Haensel, G. Keitel, N. Kosuch, U. Nielsen, and P. Schreiber, J.Phys. (France) 32, C4-236 (1971)

(50) U. Rössler, phys.stat.sol. (b) 45, 483 (1971)

(51) U. Fano and J.W. Cooper, Rev.mod.Physics 40, 441 (1968)

(52) N. Schwentner, thesis, München 1974

(53) N. Schwentner, F.-J. Himpsel, V. Saile, M. Skibowski, W. Steinmann, and E.E. Koch, Phys.Rev. Letters 34, 528 (1975)

(54) A.B. Kunz, D.J. Michish, S.K.V. Mirmira, T. Shima, F.-J. Himpsel, V. Saile, N. Schwentner, and E.E. Koch, Sol. State Commun. 17, 761 (1975)

(55) Ch. Ackermann, R. Brodmann, U. Hahn, A. Suzuki, and G. Zimmerer, phys.stat.sol. (b) 74, 579 (1976)

(56) N. Schwentner and E.E. Koch, Phys.Rev. B (1976), in press

(57) J. Jortner, L. Meyer, S.A. Rice, and E.G. Wilson, J.Chem. Phys. 42, 4250 (1965)

(58) N.G. Basov, O.V. Bogdankevich, V.A. Danylichev, A.G. Devyatkov, G.N. Kashnikov, and N.P. Lantsov, JETP Letters 7, 317 (1968)

(59) N.G. Basov, E.M. Balashov, O.V. Bogdankevitch, V.A. Danilychev, G.N. Kashnikov, N.P. Lantzov, and D.D. Khodkevitch, J. Luminesc. 1,2, 834 (1970)

(60) A. Bonnot, A.M. Bonnot, F. Coletti, J.M. Debever, and J. Hanus, J.Phys. (France) C3 35, 49 (1974)

(61) J.M. Debever, A. Bonnot, A.M. Bonnot, F. Coletti, and J. Hanus, Solid State Commun. 14, 989 (1974)

(62) J. Hanus, F. Coletti, A.M. Bonnot, and J.M. Debever, in Vacuum Ultraviolet Radiation Physics, ed. by E.E. Koch, R. Haensel, and C. Kunz, Pergamon-Vieweg, Braunschweig (1974), p.341

(63) E.E. Huber, D.A. Emmons, and R.M. Lerner, Opt. Commun. 11, 155 (1974)

(64) R.E. Packard, F. Reif, and C.M. Surko, Phys.Rev. Letters 25, 1435 (1970)

(65) J.Ya. Fugol', E.V. Savchenko, and A.G. Belov, ZhETF Pis.Red. 16, 245 (1972)

(66) A.G. Belov, J.Ya. Fugol', and E.V. Savchenko, Solid State Commun. 12, 1 (1973)

(67) J.Ya. Fugol', A.G. Belov, J.V. Savchenko, and Yu.B. Poltoratskii, Solid State Commun. 15, 525 (1974)

(68) J.Ya. Fugol', A.G. Belov, J.V. Savchenko, and Yu.B. Poltoratskii, Fiz.nizh.temp. USSR 1, 203 (1975)

(69) J.Ya. Fugol', A.G. Belov, Yu.B. Poltoratskii, and E.V. Savchenko, Fiz.nizh.temp. USSR 2, 400 (1976)

(70) M. Creuzburg and K. Teegarden, Phys.Rev. Letters 20, 593 (1968)

(71) K.J. Swyler and M. Creuzburg, J.Luminesc. 1,2, 842 (1970)

(72) M. Creuzburg, Solid State Commun. 9, 665 (1971)

(73) E. Schuberth and M.Creuzburg, phys.stat.sol. (b) 71, 797 (1975)

(74) E. Schuberth ,M. Creuzburg, and W. Müller-Lierheim, phys. stat.sol. (b) 76, 301 (1976)

(75) T. Nanba, N. Nagasawa, and M. Ueta, J.Phys.Soc. Japan 37, 1031 (1974)

(76) O. Cheshnovsky, B. Raz, and J. Jortner, J. Chem.Phys. 57, 4628 (1972)

(77) A. Gedanken, B. Raz, and J. Jortner, J.Chem.Phys. 59, 1650 (1973); J.Chem.Phys. 59, 5471 (1973)

(78) O. Cheshnovsky, B. Raz and J. Jortner, J.Chem.Phys. 59, 5554 (1973)

(79) O. Cheshnovsky, A. Gedanken, B. Raz, and J. Jortner, Solid State Commun. 13, 639 (1973)

(80) O. Cheshnovsky, A. Gedanken, B. Raz, and J. Jortner, Chem. Phys. Letters 22, 23 (1973)

(81) R. Brodmann, G. Tolkiehn, and G. Zimmerer, phys.stat.sol. (b) 73, K99 (1976)

(82) V.A. Danilychev, G.N. Kashnikov, and Yu.M. Popov, Preprint no. 136, Lebedev Institute, Moscow (1970)

(83) T. Nanba and N. Nagasawa, J.Phys.Soc. Japan 36, 1216 (1974)

(84) N. Nagasawa and T. Nanba, Optics Commun. 11, 152 (1974)

(85) R. Brodmann, R. Haensel, U. Hahn, U. Nielsen, and G. Zimmerer, Chem.Phys. Letters 29, 250 (1974)

(86) R. Brodmann, R. Haensel, U. Hahn, U. Nielsen, and G. Zimmerer, in Vacuum Ultraviolet Radiation Physics, ed. by E.E. Koch, R. Haensel, and C. Kunz, Vieweg-Pergamon, Braunschweig (1974), p.344

(87) Ch. Ackermann, R. Brodmann, G. Tolkiehn, G. Zimmerer, R. Haensel, and U. Hahn, J.Luminesc. 12/13, 315 (1976)

(88) H. Möller, R. Brodmann, and G. Zimmerer, Solid State Commun. 20 (in press)

(89) R. Brodmann, U. Hahn, G. Tolkiehn, and G. Zimmerer, unpublished results

(90) Y. Tanaka, J.Opt.Soc.Am. 45, 710 (1955)

(91) R.S. Mulliken, J.Chem.Phys. 52, 5170 (1970)

(92) M. Martin and S.A. Rice, Chem.Phys. Letters 7, 94 (1970)

(93) M. Martin, J.Chem.Phys. 54, 3289 (1971)

(94) A.G. Molchanov, Preprint no. 113, Lebedev Phys.Institute, Moscow (1970)
and Sov.Phys.Usp. 15, 124 (1972)

(95) Y. Toyozawa, in Vacuum Ultraviolet Radiation Physics, ed. by E.E. Koch, R. Haensel, and C. Kunz, Pergamon-Vieweg, Braunschweig (1974), p.263

(96) U. Hahn, N. Schwentner, and G. Zimmerer, to be published

(97) J.W. Keto, R.E. Gleason, and G.K. Walters, Phys.Rev. Letters 33, 1365 (1974)

(98) Th. Förster, Annalen der Physik 2, 55 (1948)

(99) Ch. Ackermann, thesis, Hamburg (1976)

(100) J.F. O'Brien and K.J. Teegarden, Phys.Rev. Letters 17, 919 (1966)

(101) Z. Ophir, B. Raz, and J. Jortner, Phys.Rev. Letters 33, 415 (1974)

(102) E.E. Koch, B. Raz, V. Saile, N. Schwentner, M. Skibowski, and W. Steinmann, Japan.J.Appl.Phys.Suppl. 2, Pt.2, 775 (1974)

(103) Z. Ophir, B. Raz, and J. Jortner, in Vacuum Ultraviolet Radiation Physics, ed. by E.E. Koch, R. Haensel, and C. Kunz, Pergamon-Vieweg, Braunschweig, p.350 (1974)

(104) Z. Ophir, N. Schwentner, B. Raz, M. Skibowski, and J. Jortner, J.Chem.Phys. 63, 1072 (1975)

(105) Z. Ophir, B. Raz, J. Jortner, V. Saile, N. Schwentner, E.E. Koch, M. Skibowski, and W. Steinmann, J.Chem.Phys. 62, 650 (1975)

(106) V. Saile, N. Schwentner, E.E. Koch, M. Skibowski, W. Steinmann, Z. Ophir, B. Raz, and J. Jortner, in Vacuum Ultraviolet Radiation Physics, ed. by E.E. Koch, R. Haensel, and C. Kunz, Pergamon-Vieweg, Braunschweig, p.352 (1974)

(107) D. Pudewill, F.-J. Himpsel, V. Saile, N. Schwentner, M. Skibowski, E.E. Koch, and J. Jortner, J.Chem.Phys. (1976) (in press)

(108) M.L. Klein and T.R. Koehler, in Rare Gas Solids, vol.I, ed. by M.L. Klein and J.A. Venables, Academic Press, London - New York - San Francisco (1976), p. 301

(109) N. Schwentner, M. Skibowski, and W. Steinmann, Phys.Rev. B8, 2965 (1973)

(110) N. Schwentner, to be published

(111) J.T. Devreese, A.B. Kunz, and T.C. Collins, Solid State Commun. 11, 673 (1972)

(112) E. Schuberth, thesis, Regensburg (1976)